PERGAMON

International Journal of Multiphase Flow 26 (2000) 1063–1093

International Journal of Multiphase Flow

www.elsevier.com/locate/ijmulflow

# Thermohydrodynamic characteristics of two-phase flow in a heated capillary

Y.P. Peles, L.P. Yarin, G. Hetsroni*

*Department of Mechanical Engineering, Technion — Israel Institute of Technology, Haifa, Israel*

Received 14 May 1998; received in revised form 3 July 1999

**Abstract**

Two-phase laminar flow in a heated capillary slot, driven by liquid evaporation from the interface, is investigated and a quasi-one-dimensional model is proposed. The model takes into account the multistage character of the process as well as the affect of capillarity, frictional and gravity forces on the flow development. The theoretical description of the phenomenon is based on the assumption of uniform distribution of hydrodynamic and thermal parameters over the cross-section of the liquid and vapor flows. With this approximation, the mass, thermal and momentum equations for the average parameters are obtained. These equations are solved to determine the velocity, pressure and temperature distributions along the capillary axis, the shape of the interfacial surface for various geometrical and regime parameters as well as various physical properties of the liquid and vapor. The effect of the microchannel size, initial temperature of the cooling liquid, wall heat flux and gravity on the flow are considered. 

*Keywords:* Boiling two-phase flow; Capillary slot

## 1. Introduction

The challenge posed by high electronic chip heat flux makes thermal management a key factor in the development of electronic systems. The cooling of microelectronic components by new cooling technologies, as well as improving the existing ones, is becoming a necessity as power dissipation levels of integrated circuits increase and their sizes decrease. Miniature heat

* Corresponding author.

0301-9322/00/$ - see front matter 
PII: S0301-9322(99)00082-8

sinks, in which liquid flows, in silicon wafer, could significantly improve the performance and reliability of semiconductor devices by increasing the effective thermal conductivity, decreasing the temperature gradients across the wafer, decreasing the maximum wafer temperature and reducing the number and intensity of localized hot spots.

One of the possible ways to enhance heat transfer in the cooling systems of various devices is by phase change in microchannels which are fabricated in the device. This circumstance has been the motivation for a number of theoretical and experimental investigations covering various aspects of heat transfer in a capillary space with phase change.

In the earliest research on microscale flow heat transfer, Tuckerman and Pease (1981) studied the single-phase fluid flow and heat transfer characteristics in microchannels and demonstrated that electronic chips could be effectively cooled by means of the forced convection flow of water through microchannels fabricated in the silicon. Following Tuckerman's (1984) research, some other researches (Wu and Little, 1984; Weisberg et al. 1992; Peng and Peterson, 1995) have contributed to a better understanding of the fluid flow and heat transfer mechanism occurring in microchannels with single-phase flow. An extensive review of the available cooling data for single-phase microchannels flow has been done by Bailey et al. (1995). Although single-phase microchannels can effectively cool miniature devices, they present some inherit disadvantages like large pressure drops and streamwise increases in the heat sink temperature. However, two-phase heat dissipation can achieve very high heat fluxes for a constant flow rate while maintaining a relatively constant surface temperature.

Bowers and Mudawar (1994a) performed an experimental study of boiling flow within mini-channel (2.54 mm) and micro-channel ($d = 510$ μm) heat sink and demonstrated that high values of heat flux can be achieved. Bowers and Mudawar (1994b) also modeled the pressure drop in the micro-channels and mini-channels, using Collier (1981) and Wallis (1969) homogenous equilibrium model, which assumes the liquid and vapor phases form a homogenous mixture with equal and uniform velocity and properties were assumed to be uniform within each phase.

Landerman (1994) developed an analytical model for two-phase boiling heat transfer in a high aspect ratio rectangular channel. The flow regimes in the channel were mapped and then the heat transfer and wall temperature were evaluated, using heat transfer coefficients taken from the literature.

A mathematical model of the evaporation liquid–vapor meniscus in a capillary slot has been developed by Khrustalev and Faghri (1995). The model includes a two-dimensional steady-state momentum conservation and energy equations for both the vapor and liquid phase, while the liquid–vapor interface curvature was constant along the interface. Wayner et al. (1976) developed a simple procedure to obtain the heat transfer coefficient for the interline region of an adsorption controlled wetting film. Xu and Carey (1990) developed an analytical model to predict the heat transfer characteristics of film evaporation on a microgroove surface.

A different analytical approach to the pressure drop of boiling two-phase flow in extremely narrow channels (35–110 μm between plates) was suggested by Morijama and Inoue (1992). The momentum equations for the liquid and the vapor were introduced in order to evaluate the pressure loss along the gap for slug flow and film flow regimes, assuming equal and constant liquid film thickness on the upper and lower wall.

From the foregoing literature discussion it is seen that some analytical models were

developed in order to evaluate the fluid flow and heat transfer along a capillary channel/slot. However, in order to fully understand these phenomena there is a need to develop a mathematical model which takes into consideration all the factors which influence the fluid flow and heat transfer: capillarity, frictional, inertia and gravity forces, interfacial interaction, etc.

The flow in the heated capillary depends on a number of parameters including the channel geometry, physical properties of the liquid and the heat flux. An immediate consequence of the liquid heating and evaporation is a convective motion of both phases. The latter leads to a velocity and temperature field transformation and a change in the meniscus shape.

The objective of the present research is to construct a quasi-one-dimensional model of flow in a heated capillary, with the hydrodynamic, thermal and capillarity effects. We study the influence of heat transfer on steady-state laminar flow in a heated capillary, the shape of the interface surface and the velocity and temperature distribution along the capillary axis.

In the present work, a one-dimensional model for boiling two-phase flow along a planar capillarity channel is presented. The model takes into account the affect of capillary, friction and gravity forces on the flow development and the parameters which influence the flow mechanism are evaluated. The theoretical description of the phenomena is based on the assumption of uniform parameter distribution over the cross-section of the liquid and vapor.

In the next section, we describe the physical model of the process. The governing equations and conditions of the interfacial surface are considered in Section 3 and 4. In Section 5 we present the equations for the average parameters. In Section 6, we display the quasi-one-dimensional model. The integral relations for the thermohydrodynamic characteristics of flow in a heated capillary are considered in Section 7. The results of calculations and discussion is presented in Section 8. Conclusions are summarized in Section 9.

## 2. The physical model

A capillary system is said to be in a steady-state equilibrium position when the capillary forces are equal to the hydrostatic pressure force (Levich, 1962). The heating of the capillary walls leads to a disturbance of the equilibrium and to a displacement of the meniscus, causing the liquid–vapor interface location to change as compared to an unheated wall. This process causes pressure differences due to capillarity and the hydrostatic pressures exiting the flow which in turn causes the meniscus to return into the initial position. In order to realize the above-mentioned process in a continuous manner it is necessary to carry out continual heat transfer from the capillary walls to the liquid. In this case the position of the interface surface is invariable and the fluid flow is stationary [1].

The idealized picture of the flow in a heated microchannel is shown in Fig. 1a. Such flow possesses a number of specific properties due to the existence of the interfacial surface restricting the domains filled by vapor and liquid. The latter has an infinitely thin surface with

[1] From the thermodynamical point of view the process in a heated capillary is similar to a heat engine transforming heat to mechanical energy of flow.

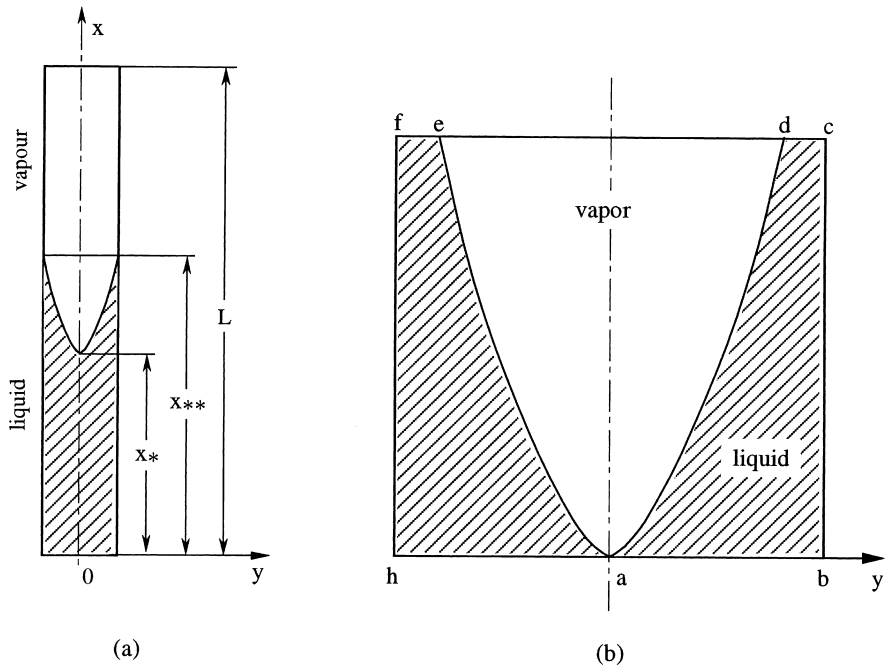


Fig. 1. (a) A heated capillary scheme. (b) The evaporation scheme. I — (a–b), II — (b–c), III — (c–d), IV — (d–a), V — (a–e), VI — (e–f), VII — (f–h), VIII — (h–a), I′ — (a–d), II′ — (e–a), III′ — (d–e)

a jump in pressure and velocity, while the temperature is equal. One can see that in a heated capillary there are three distinct regions (heated, evaporation, superheated) corresponding to different types of flow. Within the first and the third, one-phase liquid (vapor) flow occurs. Heat transfer from the wall to the fluid is accompanied by an increase of the liquid (vapor) temperature and velocity downstream. In the second region liquid–vapor flow interaction takes place. Heat flux causes the liquid to progress downstream and to evaporate.

## 3. Governing equations

The mass, thermal and momentum balance equations will be used. The key assumption of the present analysis is that the Knudsen number of the flow in the capillary is small enough. This permits one to use the continuum model for each phase. Due to the moderate flow velocity, the effects of compressibility of the phases as well as of mechanical energy dissipation in the phases are negligible. Assuming that thermal conductivity and viscosity of vapor and liquid are independent of temperature and pressure, we arrive at the following equations:

$$\mathrm{div}\rho^{(\alpha)}\boldsymbol{v}^{(\alpha)} = 0 \tag{1}$$

$$\rho^{(\alpha)}\boldsymbol{v}^{(\alpha)}\nabla h^{(\alpha)} = \lambda^{(\alpha)}\nabla^2 T^{(\alpha)} \tag{2}$$

$$\rho^{(\alpha)}(\boldsymbol{v}^{(\alpha)}\nabla)\boldsymbol{v}^{(\alpha)} = -\nabla P^{(\alpha)} + \mu^{(\alpha)}\nabla^2\boldsymbol{v}^{(\alpha)} + \frac{\mu^{(\alpha)}}{3}\text{grad div } \boldsymbol{v}^{(\alpha)} \tag{3}$$

where $\rho$, $\mathbf{v}$, $T$ and $h$ are the density, velocity, temperature and enthalpy (bold letters denote vectors) $\mathbf{v}$ has components $u$, $v$, $w$, which are directed along the axes $x$, $y$ and $z$, respectively. $P$ is the pressure, $\lambda$ and $\mu$ are the thermal conductivity and viscosity, respectively. $\nabla$ and $\nabla^2$ are the gradient and the Laplacian operator. The superscript $\alpha = 1$ and 2 corresponds to vapor ($\alpha = 1$) or liquid ($\alpha = 2$)[2].

In order to close the system of Eqs.(1)–(3) it is necessary to supplement the gas equation of state and the equation determining the dependence of liquid density on temperature

$$P^{(1)} = P^{(1)}(\rho^{(1)}T^{(1)}) \tag{4}$$

$$\rho^{(2)} = \rho^{(2)}(T^{(2)}) \tag{5}$$

The system of Eqs. (1)–(5) should also be supplemented by a correlation determining the dependence of enthalpy on temperature: $h^{(\alpha)} = h^{(\alpha)}(T^{(\alpha)})$.

## 4. Conditions of the interface surface

We now describe the conditions corresponding to the interface surface. For stationary capillarity flow, these conditions can be expressed by the equations of continuity of mass, thermal fluxes on the interface surface and the equilibrium of all acting forces (Landau and Lifshitz, 1959). For a capillary with evaporative meniscus the balance equations have the following form:

$$\sum_{\alpha=1}^{2} \rho^{(\alpha)}\boldsymbol{v}^{(\alpha)}n_i^{(\alpha)} = 0 \tag{6}$$

$$\sum_{\alpha=1}^{2} \left(\rho^{(\alpha)}\boldsymbol{v}^{(\alpha)}h^{(\alpha)} + \lambda^{(\alpha)}\frac{\partial T^{(\alpha)}}{\partial x_i}\right)n_i^{(\alpha)} = 0 \tag{7}$$

$$\sum_{\alpha=1}^{2} (P^{(\alpha)} + \rho^{(\alpha)}\boldsymbol{v}_i^{(\alpha)}\boldsymbol{v}_k^{(\alpha)})n_i^{(\alpha)} = (\sigma_{ik}^{(2)} - \sigma_{ik}^{(1)})n_k + \beta(r_1^{-1} + r_2^{-1})n_i^{(2)} + \frac{\partial\beta}{\partial x_i} \tag{8}$$

where $\beta$ is the surface tension; $\sigma_{ik}$ is the tensor of viscous tension; $\mathbf{v}^{(\alpha)}n_i^{(\alpha)}$ and $(\partial T^{(\alpha)}/\partial x_i)n_i^{(\alpha)}$ are the normal components of the velocity vector and interface surface gradient, respectively; $r_1$ and $r_2$ are the general radii of curvature of the interface surface; and $n_i$ and $n_k$ correspond to the normal and the tangent directions; $n_i^{(1)} = -n_i^{(2)}$.

When the interface surface is expressed by a function $x = \varphi(y, z)$ the general radii of

[2] The term accounting for the so-called 'second' viscosity is omitted in Eq. (3).

curvature are found from the equation (Smirnov, 1964):

$$Ar^2 + Br + c = 0 \tag{9}$$

where $A = (a_1 a_2 - a_3^2)$; $B = a_4[2a_3 a_5 a_6 - (1 + a_5^2)a_2 - (1 + a_6^2)a_1]$; $c = (1 + a_5^2 + a_6^2)^2$; $a_1 = (\partial^2 x/\partial y^2)_b$; $a_2 = (\partial^2 x/\partial z^2)_b$; $a_3 = (\partial^2 x/\partial y \partial z)_b$; $a_4 = [1 + (\partial x/\partial y)_b^2 + (\partial x/\partial z)_b^2]^{1/2}$; $a_5 = (\partial x/\partial y)_b$; $a_6 = (\partial x/\partial z)_b$. The index $b$ corresponds to the interface surface.

For the flow in a slot (the plane problem: $x = \varphi(y)$) the general radii of curvature equal

$$r_1 = \infty, \quad r_2 = \frac{(1 + f^{(1)'2})^{3/2}}{f^{(1)''}} = \psi^{-1} \tag{10}$$

where $f^{(1)'}$ and $f^{(1)''}$ equal $(\mathrm{d}f^{(1)}/\mathrm{d}x)_b$ and $(\mathrm{d}^2 f^{(1)}/\mathrm{d}x^2)_b$, respectively; $f^{(1)} = |k|y_b$ is half the vapor flow cross-section area and $k$ is a unit vector in the $z$ direction.

The vapor pressure on the interface surface may be found from the Clapeyron–Clausius equation (Appendix A):

$$\frac{\mathrm{d}P^{(1)}}{\mathrm{d}T^{(1)}} = \frac{h_{\mathrm{LG}}\rho^{(1)}}{T^{(1)}} \tag{11}$$

Assuming the vapor is an ideal gas

$$P^{(1)} = R\rho^{(1)}T^{(1)} \tag{12}$$

and combining Eqs. (11) and (12), we arrive (after integration) at the dependence of the vapor pressure on the temperature at the interface surface:

$$P^{(1)} = \tilde{P}\exp(-h_{\mathrm{LG}}/RT^{(1)}) \tag{13}$$

where $\tilde{P} = P'\exp(h_{\mathrm{LG}}/RT')$; $P'$ and $T'$ are some values of the pressure and temperature on the saturation line.

## 5. Equations for the average parameters

To derive the equations for the average parameters we use Eqs. (1)–(3) in the following form

$$\frac{\partial}{\partial x_l}(\rho^{(\alpha)}v_l^{(\alpha)}) = 0 \tag{14}$$

$$\frac{\partial}{\partial x_l}\left[(\rho^{(\alpha)}v_l^{(\alpha)}h^{(\alpha)}) - \lambda^{(\alpha)}\frac{\partial T^{(\alpha)}}{\partial x_l}\right] = 0 \tag{15}$$

$$\frac{\partial}{\partial x_k}(\Pi_{ik}^{(\alpha)}) = 0 \tag{16}$$

where $\Pi_{ik}^{(\alpha)} = P^{(\alpha)}\delta_{ik} + \rho^{(\alpha)}v_i^{(\alpha)}v_k^{(\alpha)} - \sigma_{ik}^{(\alpha)}$, $\delta_{ik}$ is the Kronecker delta; $\delta_{ik}=1$ for $i=k$, $\delta_{ik}=0$ for $i\neq k$; $i, k = 1, 2, 3$; $\sigma_{ik}^{(\alpha)}=\mu^{(\alpha)}((\partial v_i^{(\alpha)}/\partial x_k)+(\partial v_k^{(\alpha)}/\partial x_i) - (2/3)\delta_{ik}(\partial v_l^{(\alpha)}/\partial x_l))$; $l = 1, 2, 3$.

Introduce average (over the flow cross-section) parameters as:

$$\langle J^{(\alpha)}\rangle = f^{(\alpha)^{-1}}\int_{f^{(\alpha)}} J^{(\alpha)}\,\mathrm{d}s \tag{17}$$

where $J$ is the parameter under examination and $\langle\ \rangle$ is the operator indicating averaging over the cross-section. Then we obtain equations for the average parameters (Appendix B).

These equations, supplemented by the expression for the liquid density and vapor pressure, may be integrated for the general case only numerically. However, for some important particular cases, reasonable approximations can be introduced which simplify the system of equations for the average parameters to a form that can be integrated analytically. This approach, developed below, yields expressions for a set of first order integral equations of the average parameters.

## 6. Quasi-one-dimensional approach

Significant simplification of the governing equations may be achieved by using a quasi-one-dimensional model for the flow. Assuming: (i) the velocity, temperature and pressure distributions in the cross-section are uniform, (ii) all parameters depend on longitudinal coordinate and expressing the external heat flux and drag force as $Q_{\mathrm{ext}} = \int_{f_{ii}} q\,\mathrm{d}s$, $F_{\mathrm{ext}} = \int_{f_{ii}} t\,\mathrm{d}s$ ($f_{ii}=|k|\int_{x_{\mathrm{in}}}^{x}\mathrm{d}x$, $f_{\mathrm{int}}=|k|\int_{x_{in}}^{*}[1+(f^{(1)})^2]^{1/2}$), ($x_{in}$ is some initial value of $x$) we obtain the following equations:

$$\frac{\mathrm{d}}{\mathrm{d}\bar{x}}\left(\sum_{\alpha=1}^{2}\bar{\rho}^{(\alpha)}\bar{u}^{(\alpha)}\bar{f}^{(\alpha)}\right) = 0 \tag{18}$$

$$\frac{\mathrm{d}}{\mathrm{d}\bar{x}}\left(\sum_{\alpha=1}^{2}\bar{\rho}^{(\alpha)}\bar{u}^{(\alpha)}\bar{h}^{(\alpha)}\bar{f}^{(\alpha)}\right) = \vartheta + Pe^{-1}\sum_{\alpha=1}^{2}\bar{\lambda}^{(\alpha)}\frac{\mathrm{d}}{\mathrm{d}\bar{x}}\left(\bar{f}^{(\alpha)}\frac{\mathrm{d}\bar{T}}{\mathrm{d}\bar{x}}\right) \tag{19}$$

$$\begin{aligned}&\frac{\mathrm{d}}{\mathrm{d}\bar{x}}\left(\sum_{\alpha=1}^{2}\bar{\rho}^{(\alpha)}\bar{u}^{(\alpha)^2}\bar{f}^{(\alpha)}\right) + Eu\frac{\mathrm{d}}{\mathrm{d}\bar{x}}\left(\sum_{\alpha=1}^{2}\bar{P}^{(\alpha)}f^{(\alpha)}\right)\\ &\quad= \frac{\mathrm{d}}{\mathrm{d}\bar{x}}\bar{F}_{\mathrm{ext}} + Re^{-1}\frac{\mathrm{d}}{\mathrm{d}\bar{x}}\left(\sum_{\alpha=1}^{2}\bar{\mu}^{(\alpha)}\bar{\sigma}^{(\alpha)}\bar{f}^{(\alpha)}\right) - We^{-1}\frac{\mathrm{d}}{\mathrm{d}\bar{x}}\left(\int_{\bar{f}_{\mathrm{int}}}\bar{\beta}\bar{\psi}n_i^{(2)}\,\mathrm{d}\bar{S}\right)\\ &\quad- We^{-1}\frac{\mathrm{d}}{\mathrm{d}\bar{x}}\left(\int_{\bar{f}_{\mathrm{int}}}\frac{\partial\bar{\beta}}{\partial\bar{x}_i}\,\mathrm{d}\bar{S}\right) + Fr^{-1}\int_{\bar{f}^{(\alpha)}}\left(\sum_{\alpha=1}^{2}\bar{X}^{(\alpha)}\right)\mathrm{d}\bar{S}\end{aligned} \tag{20}$$

$$\frac{\mathrm{d}}{\mathrm{d}\bar{x}}(\bar{\rho}^{(\alpha)}\bar{u}^{(\alpha)}\bar{f}^{(\alpha)}) = \frac{\mathrm{d}}{\mathrm{d}\bar{x}}\bar{G}_{\mathrm{int}}^{(\alpha)} \tag{21}$$

$$\frac{\mathrm{d}}{\mathrm{d}\bar{x}}(\bar{\rho}^{(\alpha)}\bar{u}^{(\alpha)^2}\bar{f}^{(\alpha)}) + Eu\frac{\mathrm{d}}{\mathrm{d}\bar{x}}(\bar{P}^{(\alpha)}\bar{f}^{(\alpha)}) = \frac{\mathrm{d}\bar{F}_{\mathrm{ext}}^{(\alpha)}}{\mathrm{d}\bar{x}} + Re^{-1}\frac{\mathrm{d}}{\mathrm{d}\bar{x}}(\bar{\mu}^{(\alpha)}\bar{\bar{\sigma}}^{(\alpha)}\bar{f}^{(\alpha)}) - \frac{\mathrm{d}\bar{F}_{\mathrm{int}}^{(\alpha)}}{\mathrm{d}\bar{x}} + Fr^{-1}\int_{\bar{f}^{(\alpha)}}\bar{X}^{(\alpha)}\,\mathrm{d}\bar{S} \tag{22}$$

$$\sum_{\alpha=1}^{2}\bar{f}^{(\alpha)} = 1 \tag{23}$$

where the characteristic scales: pressure $P_{20}$, density $\rho_{20}$, velocity $\mathrm{u}_{20}$, temperature $T_{20}$, heat capacity $c_{\mathrm{p}20}$, viscosity $\mu_{20}$, thermal conductivity $\lambda_{20}$, surface tension $\beta_{20}$ ($\beta_{20}$ corresponds to $T_{20}$), area $f$, length $d$ ($d$ is half of the capillary width), are used to define the following dimensionless parameters: $\bar{P}^{(\alpha)} = P^{(\alpha)}/P_{20}$; $\bar{\rho}^{(\alpha)} = \rho^{(\alpha)}/\rho_{20}$; $\bar{\rho}^{(\alpha)} = \rho^{(\alpha)}/\rho_{20}$; $\bar{u}^{(\alpha)} = u^{(\alpha)}/u_{20}$; $\bar{T} = T^{(\alpha)}/T_{20}$; $\bar{c}_p^{(\alpha)} = c_p^{(\alpha)}/c_{p_{20}}$; $\bar{\mu}^{(\alpha)} = \mu/\mu_{20}$; $\bar{\lambda}^{(\alpha)} = \lambda^{(\alpha)}/\lambda_{20}$; $\bar{\beta}^{(\alpha)} = \beta/\beta_{20}$; $\bar{f}^{(\alpha)} = f^{(\alpha)}/f$; $\bar{s} = s/f$; $\bar{x} = x/d$; $\bar{F} = F/\rho_{20}u_{20}^2 f$; $\bar{G} = G/\rho_{20}u_{20} f$; $\bar{\psi} = \psi d$.

$Re = u_{20}d/\nu_{20}$; $Eu = P_{20}/\rho_{20}u_{20}^2$; $Fr = u_{20}^2/gd$; $Pe = u_{20}d\rho_{20}c_{p_{20}}/\lambda_{20}$; $We = d\rho_{20}u_{20}^2/\beta_{20}$ are the Reynolds, the Euler, the Froude, the Peclet and the Weber numbers; $\vartheta = q/\rho_{20}u_{20}c_{p_{20}}T_{20}$.

The dimensionless forms of Eqs.(5), (12), (13) and (23) are

$$\bar{\rho}^{(2)} = \bar{\rho}^{(2)}(\bar{T}^{(2)}) \tag{24}$$

$$Eu\bar{P}^{(1)} = \gamma\bar{\rho}^{(1)}\bar{T}^{(1)} \tag{25}$$

$$Eu\bar{P}^{(1)} = \Omega\exp(-\omega/\bar{T}^{(1)}) \tag{26}$$

$$\sum_{\alpha=1}^{2}\bar{f}^{(\alpha)} = 1 \tag{27}$$

where $\gamma = \mathrm{RT}_{20}/\mathrm{u}_{20}^2$; $\omega = \mathrm{q}_{\mathrm{ev}}/\mathrm{RT}_{20}$; $\Omega = \tilde{P}/\rho_{20}u_{20}^2$.

Under characteristic conditions of the capillarity flow, the non-dimensional groups have the following orders: $Re \sim 1$, $Pe \sim 10$, $Eu \sim 10^7$, $Fr \sim 10^{-3}$, $We \sim 10^{-4}$, $\vartheta \sim 1$[3]. So $\bar{\lambda}^{(1)} \sim 10^{-1}$, $\bar{\lambda}^{(2)} = 1$, $\bar{\mu}^{(1)} \sim 10^{-2}$, $\bar{\mu}^{(2)} = 1$, $\bar{u}^{(1)} \sim 10^3$, $\bar{u}^{(2)} = 1$, $\bar{P}^{(\alpha)} \sim 1$, $\bar{T} \sim 1$, $\bar{f}^{(\alpha)} \sim 1$, $\bar{x} \sim 1$, the order of magnitude of the derivatives in Eqs. (19)–(22) is 1[4]. Accordingly, it is possible to omit the first term in the left hand side of Eqs.(20) and (22) and the second term in the right hand side. At moderate and large heat fluxes on the wall ($q > 10$ w/m$^2$), the first terms in the left hand side

[3] For water flow in a heated capillary with $d = 5 \times 10^{-4}$ m at $u = 10^{-3}$–$10^{-2}$ m/s and $q = 10^6$ w/m$^2$.

[4] Within the heating and superheat regions $\bar{x} \gg 1$ derivatives in Eqs. (19)–(22) are 0(1).

and right hand side of Eq. (19) are of the same order. In this case it is possible to omit the second term in the right hand side of Eq. (19).

## 7. Integral relations

The integral relations for the present problem have the following form (Appendix C).

### 7.1. Heating region: $0 \le \bar{x} \le \bar{x}_*$, $\bar{f}^{(1)} = 0$, $\bar{f}^{(2)} = 1$

$$\bar{\rho}^{(2)}\bar{u}^{(2)} = 1 \tag{28}$$

$$\bar{T}^{(2)} = 1 + \vartheta\bar{x} \tag{29}$$

$$(\bar{u}^{(2)} - 1) + Eu(\bar{P}^{(2)} - 1) = -\bar{x}(32/Re + \bar{\rho}^{(2)}/Fr) \tag{30}$$

### 7.2. Evaporation region: $\bar{x}_* \le \bar{x} \le \bar{x}_{**}$

Equations (18)–(22) have the following integrals

$$\sum_{\alpha=1}^{2} (\bar{\rho}^{(\alpha)}\bar{u}^{(\alpha)}\bar{f}^{(\alpha)}) = 1 \tag{31}$$

$$\sum_{\alpha=1}^{2} (\bar{\rho}^{(\alpha)}\bar{u}^{(\alpha)}\bar{f}^{(\alpha)}\bar{h}^{(\alpha)}) = \bar{h}_*^{(1)} + \vartheta(\bar{x} - \bar{x}_*) \tag{32}$$

$$\begin{aligned}\sum_{\alpha=1}^{2}(\bar{\rho}^{(\alpha)}\bar{u}^{(\alpha)^2}f^{(\alpha)}) + Eu\sum_{\alpha=1}^{2}\left(\bar{P}^{(\alpha)}\bar{f}^{(\alpha)}\right) &= \bar{F}_{\text{ext}} - We^{-1}\int_{\bar{f}_{\text{int}}} \bar{\beta}\bar{\psi}n_i \,\mathrm{d}\mathbf{S} - We^{-1}\int_{\bar{f}_{\text{int}}} \frac{\partial\beta}{\partial\bar{x}_i} \\ \mathrm{d}\mathbf{S} - Fr^{-1}\int_{\bar{x}_*}^{\bar{x}}\left(\sum_{\alpha=1}^{2}\bar{\rho}^{(\alpha)}\bar{f}^{(\alpha)}\right)\mathrm{d}\bar{x} &+ Eu\bar{P}_*^{(2)} + \bar{\rho}_*^{(2)}u_*^{(2)^2} - 32/Re\bar{x}_*\end{aligned} \tag{33}$$

$$\bar{\rho}^{(1)}\bar{u}^{(1)}\bar{f}^{(1)} = \int_{\bar{x}_*}^{\bar{x}} \bar{\rho}^{(1)}\bar{u}^{(1)}\sqrt{1 + (f^{(1)'})^2}\,\mathrm{d}\bar{x} \tag{34}$$

$$\bar{\rho}^{(1)}\bar{u}^{(1)^2}\bar{f}^{(1)} + Eu\bar{P}^{(1)}\bar{f}^{(1)} = \int_{\bar{x}_*}^{\bar{x}} (Eu\bar{P}^{(1)} + \bar{\rho}^{(1)}\bar{u}^{(1)^2})\sqrt{1+(f^{(1)'})^2}\,\mathrm{d}x - Fr\int_{\bar{x}_*}^{\bar{x}} \bar{\rho}^{(1)}\bar{f}^{(1)}\,\mathrm{d}\bar{x} \tag{35}$$

### 7.3. Superheat region: ($\bar{f}^{(1)} = 1; \bar{f}^{(2)} = 0$)

Equations (18)–(20) have the following integrals

$$\bar{\rho}^{(1)}\bar{u}^{(1)} = 1 \tag{36}$$

$$\bar{\rho}^{(1)}\bar{u}^{(1)}\bar{h}^{(1)} = \bar{\vartheta}\bar{x} + \bar{c}_p^{(1)}\bar{T}_{**}^{(1)} - \vartheta\bar{x}_{**} \tag{37}$$

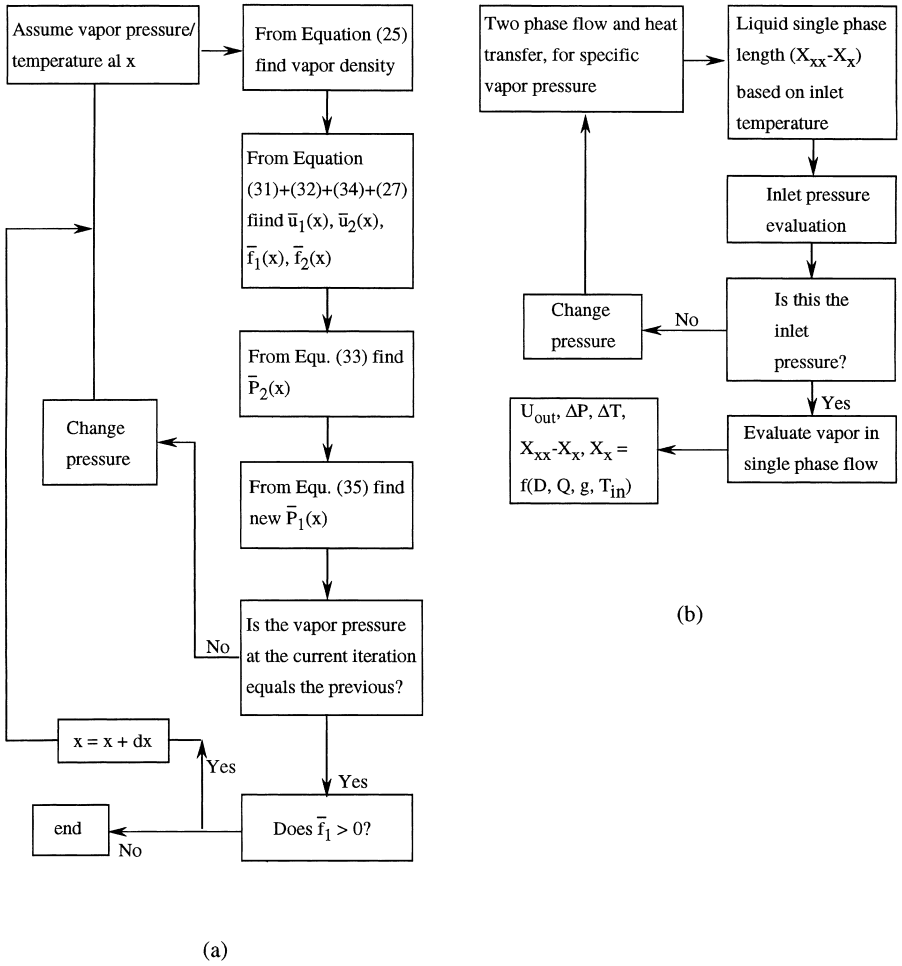


Fig. 2. The scheme of the numerical solution procedure. (a) Two-phase region. (b) Entire flow domain.

$$(\bar{u}^{(1)} - \bar{u}^{(1)}_{**}) + Eu(\bar{P}^{(1)} - \bar{P}^{(1)}_{**}) = -32/Re(\bar{x} - \bar{x}_{**}) - Fr^{-1}(\bar{\rho}^{(1)}\bar{x} - \bar{\rho}^{(1)}_{**}\bar{x}_{**}) \quad (38)$$

## 8. Results and discussion

### 8.1. Parametrical study

The numerical solution of Eqs. (18)–(27) was carried out for laminar flow, for a set of non-dimensional groups varying within the limits: $5 \times 10^8 \leq Eu \leq 10^{12}$; $1 < \vartheta < 10^{+3}$; $5 \times 10^{-10} \leq$

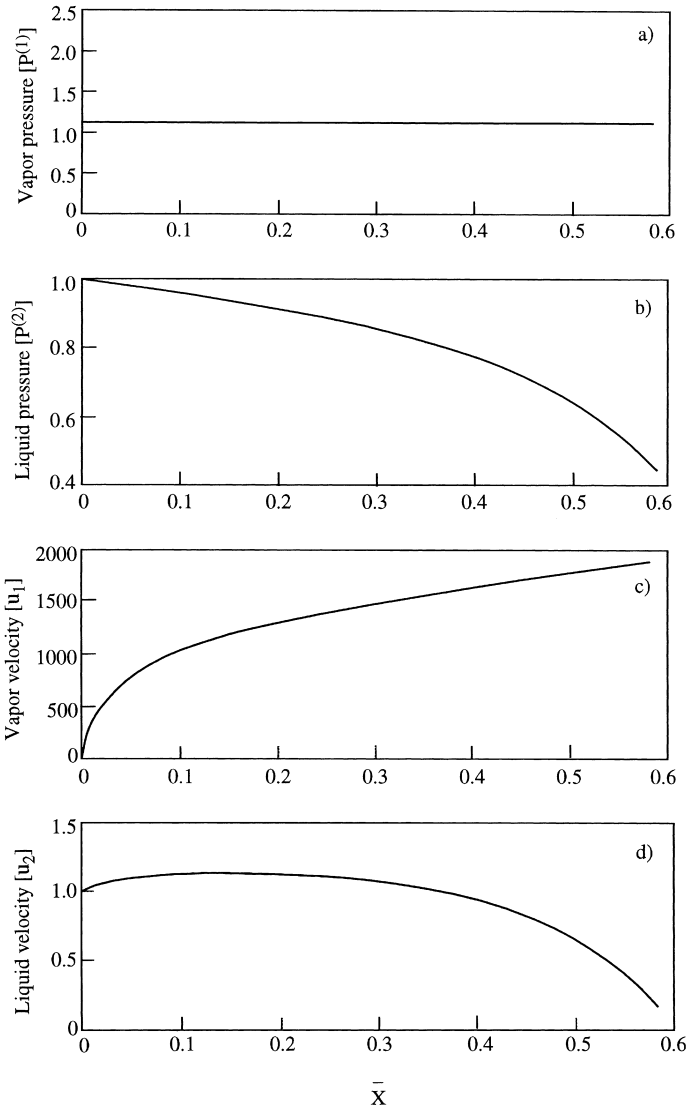


Fig. 3. The vapor and liquid pressure and velocity distribution within the evaporation region. for $We = 10^{-9}$, $\vartheta = 2.5$, $Eu = 1.6 \times 10^{11}$, $Re = 0.04$, $Fr = 1.3 \times 10^{-7}$.

$We \leq 10^{-6}$; $5 \times 10^{-3} \leq Re \leq 10$; $10^{-8} \leq Fr \leq 10^{-2}$. The non-dimensional groups were chosen based on water flow in a 500 μm slot, heat flux variation of 1 (w/cm$^2$) to 100 (w/cm$^2$) and $10^{-5}$ (m/s) $\leq u_{20} \leq 2 \times 10^{-1}$ (m/s) velocity variation. Figure 2a shows schematically the numerical solution procedure for the two-phase domain.

The calculations show that the liquid pressure monotonically decreases along the heating region. Within the evaporation region a noticeable difference between the vapor and liquid pressures takes place. The latter is connected with the effect of Laplace force due to the curvature of the interphase surface. In the superheated region the vapor pressure decreases downstream.

Figure 3a and b shows the character of the liquid and the vapor pressure distribution along the evaporation region. It is found that for the above-mentioned parameters, the vapor pressure is practically independent on $x$. Accordingly, the vapor temperature, as well as the density, are also approximately constant. The latter makes it possible to reduce the number of equations by 3. The remaining five equations consist of four equations that contained only

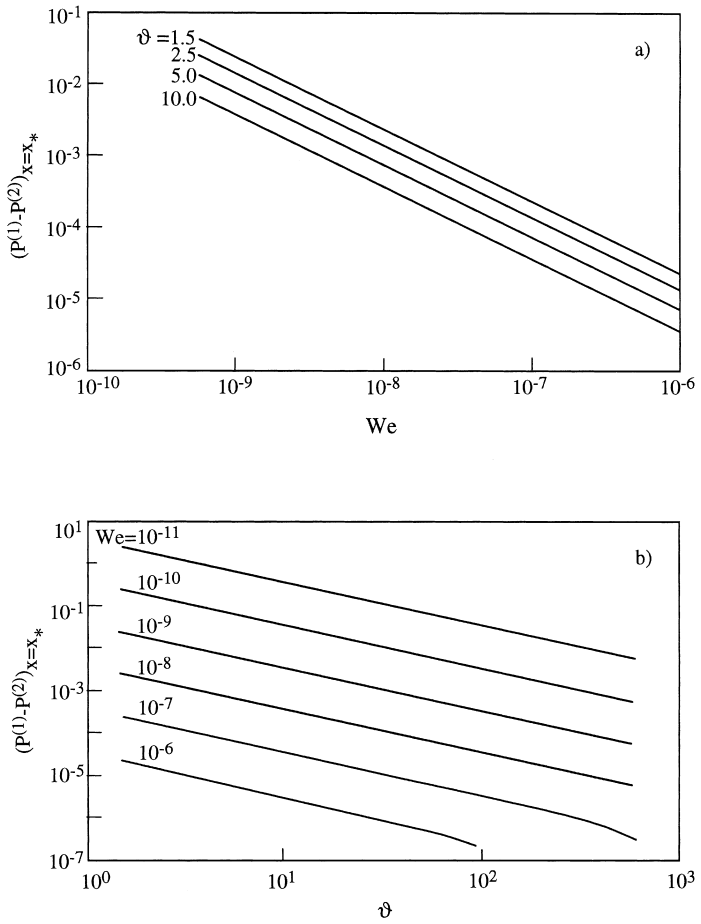


Fig. 4. The dependences $\Delta P$ ($We$) and $\Delta P$ ($\vartheta$) for different $\vartheta$ at $x_*$, for $Eu = 1.6 \times 10^{11}$, $Re = 0.04$, $Fr = 10^{-6}$.

four unkowns ($u^{(1)}$, $u^{(2)}$, $f^{(1)}$, $f^{(2)}$) and one equation (the combined vapor–liquid momentum balance) which contains the additional unknown $P^{(2)}$. That means that the system of governing equations may be solved successively: at first to get $u^{(1)}$, $u^{(2)}$, $f^{(1)}$, $f^{(2)}$ and then to get $P^{(2)}$ by solving the equation for the total momentum. Note that $u^{(1)}$, $u^{(2)}$, $f^{(1)}$, $f^{(2)}$ depend on $\vartheta$ and $P^{(1)}$ which is a function of the other non-dimensional groups: $P^{(1)}=f(Eu, Re, Fr, We)$. The liquid pressure decreases along the evaporation region and a sharp drop takes place near the top of the evaporation region.

The liquid and vapor velocity versus axial position for the evaporation region are shown in Fig. 3c and d. It is seen that the vapor velocity increases as $\bar{x}^{0.4}$, whereas the liquid velocity is

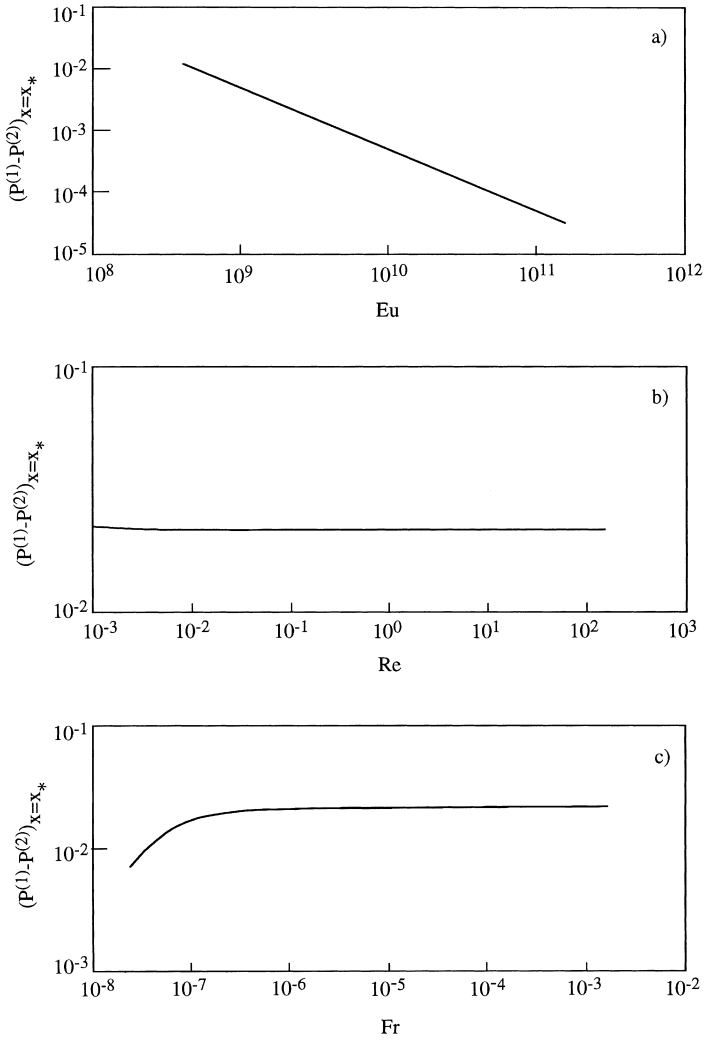


Fig. 5. (a) The dependence $\Delta P$ ($Eu$) at $x_*$, for $We = 10^{-7}$, $\vartheta = 10$, $Re = 0.1$, $Fr = 10^{-7}$. (b) The dependence $\Delta P$ ($Re$) at $X_*$, for $We = 10^{-7}$, $\vartheta = 10$, $Eu = 2.5 \times 10^{8}$, $Fr = 10^{-5}$. (c) The dependence $\Delta P$ ($Fr$) at $X_*$, for $We = 10^{-7}$, $\vartheta = 10$, $Eu = 2.5 \times 10^{8}$, $Re = 0.1$.

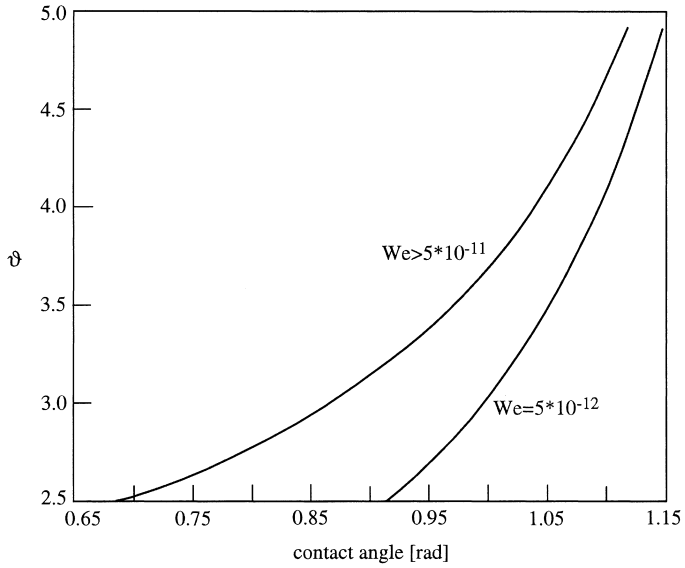


Fig. 6. The correlations $\vartheta(\Theta)$ for different *We* numbers.

almost constant along a wide range of $\bar{x}$ and decreases very sharply towards the top of the evaporation region.

The effect of various parameters on difference pressure between vapor and liquid is illustrated in Figs. 4 and 5. It is seen that the effect of the Euler and Weber numbers as well as the thermal parameter $\vartheta$ is highly noticeable. An increase in *Eu*, *We* and $\vartheta$ leads to a decrease

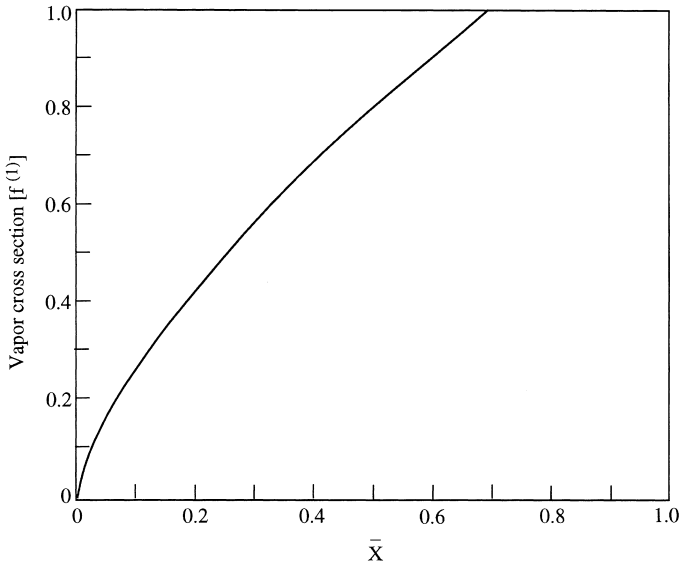


Fig. 7. The shape of interface surface for $We = 10^{-7}$, $\vartheta = 2.5$, $Eu = 1.6 \times 10^{11}$, $Fr = 10^{-7}$, $Re = 0.04$.

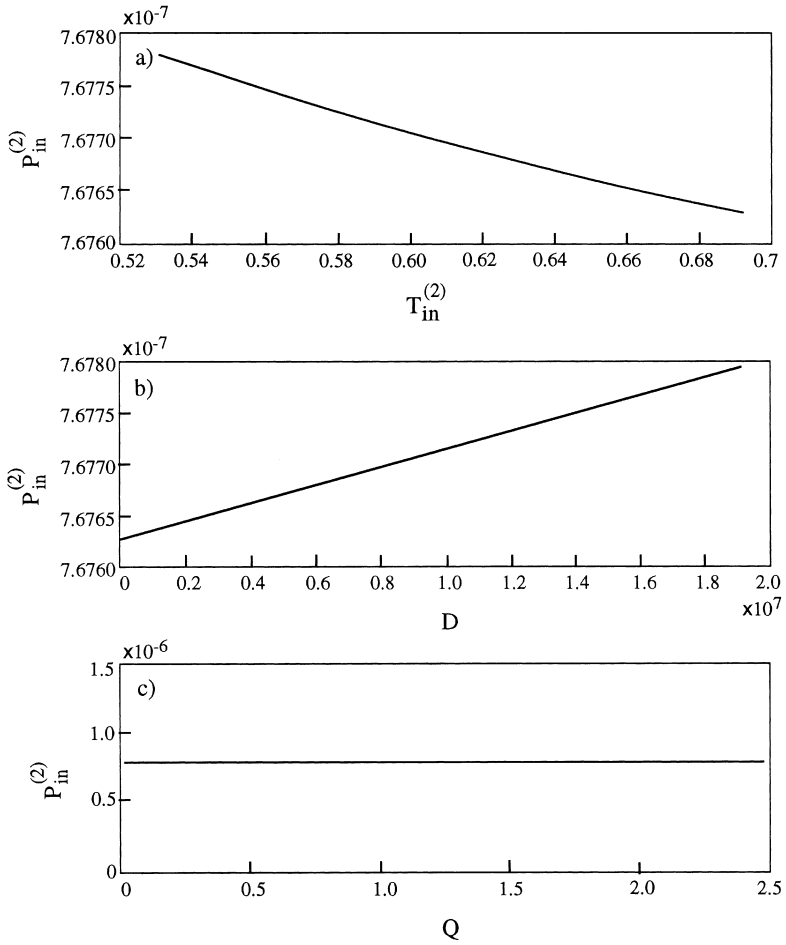


Fig. 8. The effect of inlet liquid temperature, gap-size and wall heat flux on the inlet cross-section pressure of the microchannel.

in $\Delta P$, whereas the difference of both phase pressures is practically independent of Reynolds number. An increase in the Froude number is accompanied by an increase in $\Delta P$ for a small $Fr$. At $Fr > 10^{-6}$ the effect of $Fr$ on $\Delta P$ is negligible.

The $\vartheta(\Theta)$ correlation corresponding to various Weber numbers is shown in Fig. 6. The shape of the interface surface in a capillary flow with phase change is presented in Fig. 7. As the calculations show, the curvature of the meniscus is not constant and grows toward the periphery.

### 8.2. The effect of regulated parameters

The regulated parameters of the problem are: the width and length of microchannel $\bar{d} = dh_{LG}\rho^{(2)}/\beta$ and $\bar{L} = Lh_{LG}\rho^{(2)}/\beta$, initial temperature of the liquid $\bar{T}^{(2)}_{inl} = T^{(2)}_{inl}c^{(2)}_p/h_{LG}$, gravity

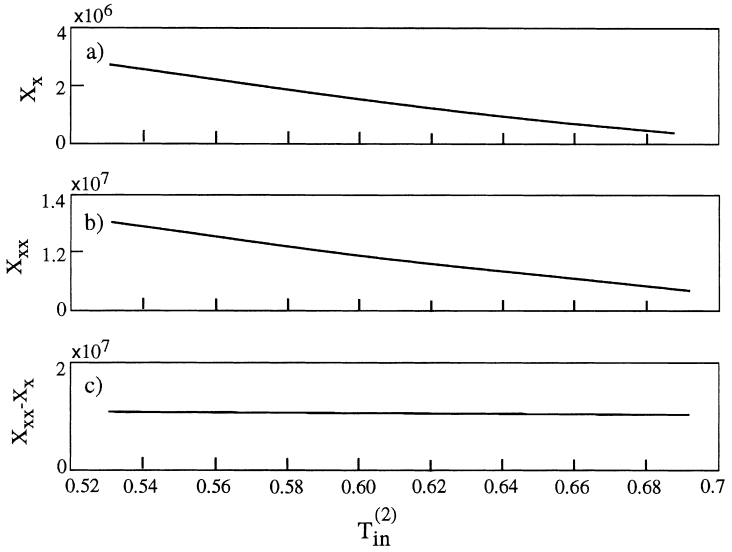


Fig. 9. The effect of inlet liquid temperature on the meniscus position (a) the dependence of $x_*(T_{\mathrm{inl}}^{(2)})$; (b) the dependencies of $x_{**}(T_{\mathrm{inl}}^{(2)})$; (c) the dependencies of $\Delta x(T_{\mathrm{inl}}^{(2)})$.

acceleration $\bar{g} = g\beta^3/\nu^{(2)^2}h_{\mathrm{LG}}^{(2)^3}$ and heat flux on the wall $\bar{q} = (q\beta/\rho^{(2)^2}h_{\mathrm{LG}}\nu^{(2)}$. The effect of these parameters on the flow characteristics: the liquid and vapor velocities $\bar{u}^{(i)} = u^{(i)}\beta/\nu^{(2)}h_{\mathrm{LG}}\rho^{(2)}$, temperatures $\bar{T}^{(i)} = T^{(i)}c_p^{(2)}/h_{\mathrm{LG}}$, pressures $\bar{p}^{(i)} = p^{(i)}/\rho^{(2)^3}(\nu^{(2)}h_{\mathrm{LG}}/\beta)^2$ and the length of the heating and evaporation region $\bar{x}_j = x_j h_{\mathrm{LG}}\rho^2/\beta$ was studied numerically.

The subsequent calculations were performed for laminar flow of water ($\rho^{(2)} = 10^3$ kg/m$^3$, $c_{\mathrm{p}} = 4.19$ kJ/kg K, $\beta = 0.059$ N/m, $h_{\mathrm{LG}} = 2256$ kJ/kg, $\theta = 0.67$ rad) in a vertical slot of height $d = 1.5$ mm. The inlet water temperature $T_{\mathrm{inl}}^{(2)}$, gap-size $d$, heat flux $q$ and acceleration due to gravity $g$ were varied within the limits; $273 < T_{\mathrm{inl}}^{(2)} < 373$ (K), $1 < d < 500$ (μm), $10 < q < 600$ (W/cm$^2$), $1 < g < 600$ (m/s$^2$). Figure 2b shows schematically the numerical solution for the entire flow domain (i.e. the liquid single-phase flow, two-phase flow and super heated single-phase vapor flow). *dt* begin with the evaluation in the two-phase domain for initial guess of the vapor pressure at the beginning of this domain ($x_*$). The liquid single-phase length $x_*$ is obtained based on the inlet temperature and the inlet pressure is calculated. If it is the inlet pressure, the properties of the single-phase flow in the liquid and vapor domain are calculated and the numerical evaluation ends, if not the vapor pressure at $x_*$ in the two-phase domain is changed and another iteration takes place. The calculations show that $P_{\mathrm{inl}}^{(2)}$, for a fixed vapor evaporation pressure, depends very weakly on $T_{\mathrm{inl}}^{(2)}$, $d$ and $q$ at large Euler numbers. For example, the variation of $\bar{T}_{\mathrm{inl}}^{(2)}$, $\bar{d}$ and $\bar{q}$ within the limits $0.52 \le \bar{T}_{\mathrm{inl}}^{(2)} \le 0.68$, $4 \times 10^4 \le \bar{d} \le 2 \times 10^7$; $10^{-8} \le \bar{q} \le 2.5 \times 10^{-7}$ corresponds (at $Eu > 10^8$) to less than 0.02% change in $P_{\mathrm{inl}}^{(2)}$ (Fig. 8). The temperature in the meniscus symmetry point $T_{20}$ equals the saturation temperature $T_{\mathrm{s}}$. Since the pressure drop in the liquid region of the capillary flow is small, it is possible to assume that $T_{\mathrm{s}}$ corresponds to $P_{\mathrm{out}}^{(1)}$ The estimations show that such assumption does not effect practically, the results of the calculations.

The effect of the inlet liquid temperature, the size of the capillary gap, the wall heat

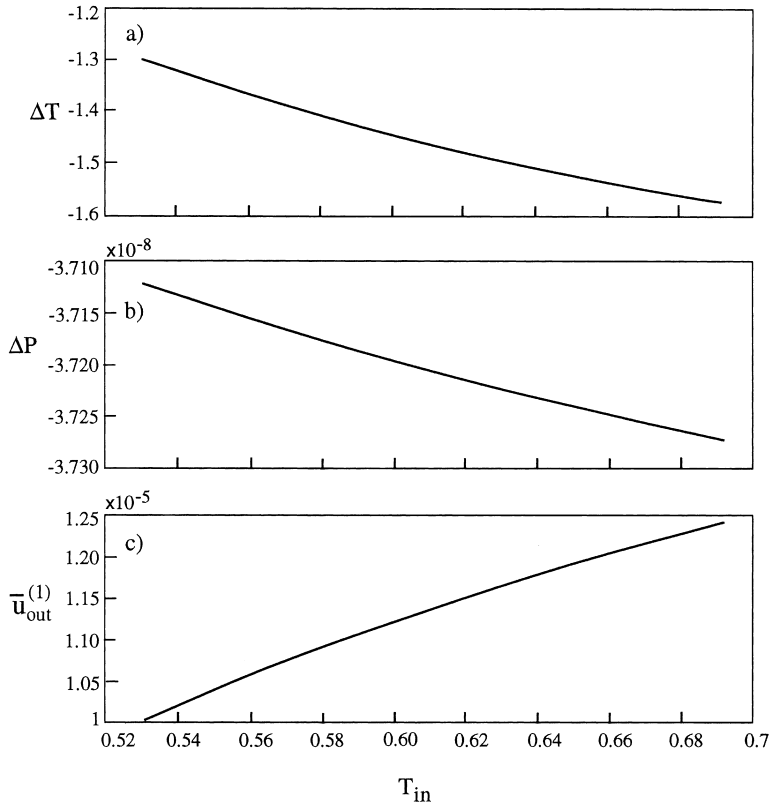


Fig. 10. The dependencies of vapor temperature, pressure and velocity in the outlet cross-section of the capillary on the inlet liquid temperature (a) the dependence of $\Delta p(T_{\mathrm{inl}}^{(2)})$; (b) the dependence of $\Delta x(T_{\mathrm{inl}}^{(2)})$; (c) the dependence of $u^{(1)}(T_{\mathrm{inl}}^{(2)})$.

flux and gravity on the hydrodynamic and the thermal characteristics of the flow in microchannel are illustrated in Figs. 8–16. These data show that the preliminary heating of the liquid (increase of $T_{\mathrm{inl}}^{(2)}$) is accompanied by displacement of the meniscus toward the inlet of capillary. In accordance with that the length of the liquid region of the flow ($x_*$) decrease whereas the length of vapor region increase. Noteworthy that the length of the evaporation region (as well as the shape of interface surface) does not depend on $T_{\mathrm{inl}}^{(2)}$.

Expansion of the vapor region leads to a vapor temperature and velocity growth at the outlet. (Fig.10a–c). The latter is accompanied by a significant change of the microchannel drag. The calculation has shown that the decrease in the liquid region drag is smaller than the growth of the hydraulic drag at the vapor region. As a consequence the total pressure drop between the inlet and outlet cross-sections of the microchannel increase as the liquid preliminary heating increases (Fig. 10b).

The effect of capillary gap-size on the interface surface, vapor velocity and the difference of pressure and temperature between inlet and outlet cross-sections of the microchannel is illustrated in Figs. 11 and 12. It is seen that an increase in $d$ leads to the expansion of the

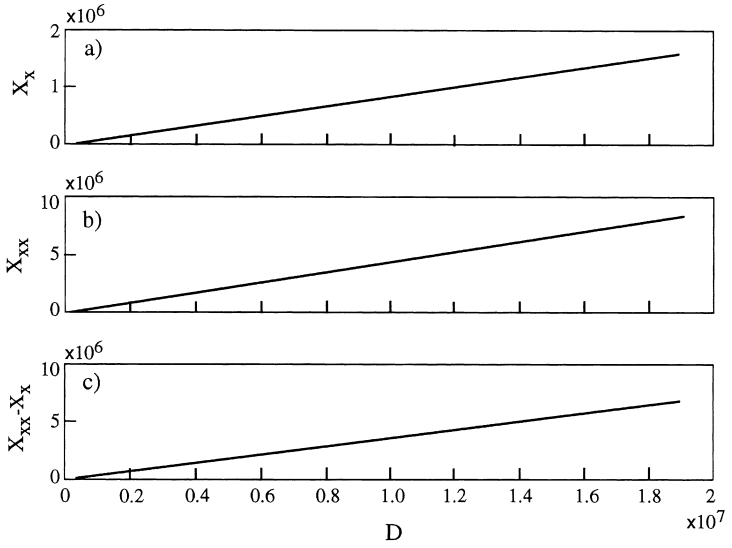


Fig. 11. The effect of gap-size on the meniscus position (a) the dependence of $x_*$(d); (b) the dependence of $x_{**}$(d); (c) the dependence of $\Delta x(d)$.

liquid region. This effect is explained as follows: at the fixed values of the other parameters an increase of $d$ leads to a growth in the total mass flux of the liquid through the capillary. Since the area of heat transfer surface and wall heat flux are invariable, the energy per unit mass of liquid decrease. Accordingly the heating rate of the liquid decreases too. The latter is accompanied by a displacement of the meniscus toward the outlet cross-section and therefore $x_*$ increases. The length of the evaporation region increase proportionally to the size of the gap, whereas the $(x_{**}-x_*)/d$ ratio does not depend on $d$. The latter shows that the shape of the interface surfaces are similar for various $d$. The decrease of the superheat region length with gap-size growth leads to a decrease in the outlet vapor velocity and temperature (Fig. 12).

The effect of gravity on the liquid and vapor parameters in the inlet and outlet cross-section is presented in Figs. 13 and 14. It is seen that an increase in the gravity is accompanied by a significant growth of the liquid pressure $P_{\mathrm{inl}}^{(2)}$ (Fig. 13a). At the same time an increase of the vapor pressure in the outlet cross-section is observed. However, the rate of liquid and vapor pressure growth are very different. This causes an increase of the difference $\Delta p = p_{\mathrm{inl}}^{(2)} - p_{\mathrm{out}}^{(1)}$ as gravity increase as well as the sign change at some value of $\bar{g}$. The temperature difference $\Delta T = T_{\mathrm{inl}}^{(2)} = T_{\mathrm{out}}^{(1)}$ and vapor velocity in the outlet cross-section of the microchannels practically do not depend on gravitational acceleration. (Fig. 14).

The effect of wall heat flux on the length of the heating and evaporation regions, vapor velocity, temperature and pressure in the outlet cross-section is shown in Figs. 14–16. These data illustrate some important features of capillary flow at large Euler numbers.

As was shown earlier at $Eu > 10^8$ the mass flux through the microchannels is directly proportional to the wall heat flux. In this case the energy per unit mass of liquid absorbed from the wall does not depend on the value of the heat flux. As a consequence the length of the heating and evaporation regions as well as the liquid and vapor temperatures are invariable

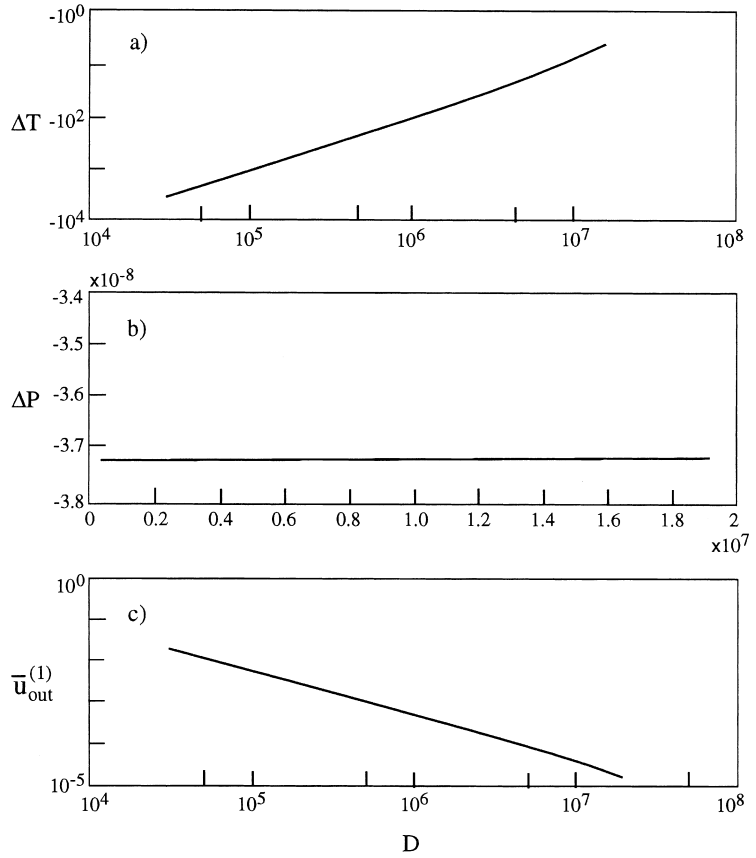


Fig. 12. The dependence of vapor temperature, pressure and velocity on gap-size (a) the dependence of $\Delta T(d)$; (b) the dependence of $\Delta p(a)$; (c) the dependence of $u^{(1)}(d)$.

on $q$. This phenomenon which may be called "the effect of self-regulation" has an important meaning to estimate the limiting permissible thermal states of the system with phase change of a cooling liquid. Ha and Peterson (1998) and Peterson and Ha (1998) showed that for V-shape micro-grooves, the evaporation length decreases slightly as heat flux increases. However, the Euler number in this research is of the order of $10^7$ ($Eu < 10^8$) and the capillary pumping mechanism in this kind of geometry is primarily due to the receding radius of curvature parallel to the flow direction.

At $Eu > 10^8$ the wall temperature $T_w$ depends on the liquid (vapor) temperature, the heat transfer intensity and the wall heat flux.

To estimate the limiting permissible value of the wall heat flux we use the thermal balance equation

$$\alpha \Delta T = q \tag{39}$$

where $\alpha$ is the convection heat transfer coefficient, $\Delta T = T_w - T^{(1)}$.

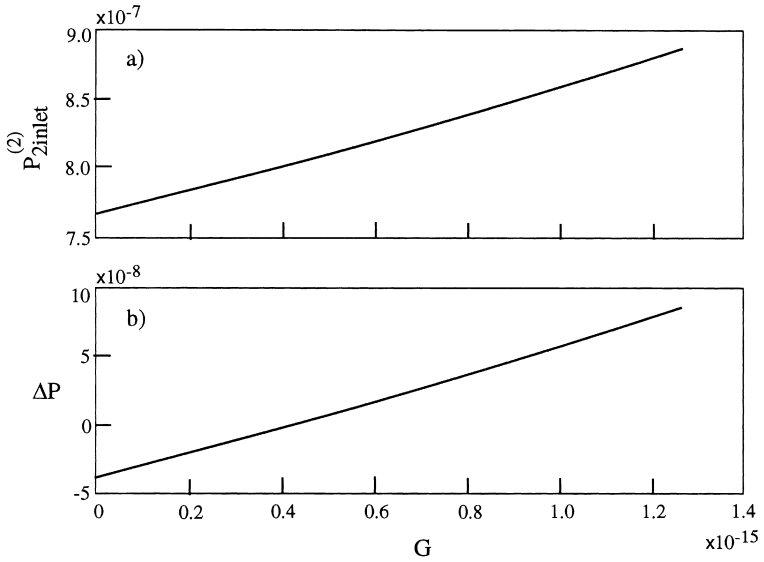


Fig. 13. The effect of gravity on inlet liquid pressure and pressure difference between the inlet and outlet cross-section of the capillary. (a) the dependence of $P_{\mathrm{inl}}^{(2)}(g)$; (b) the dependence of $\Delta P(g)$.

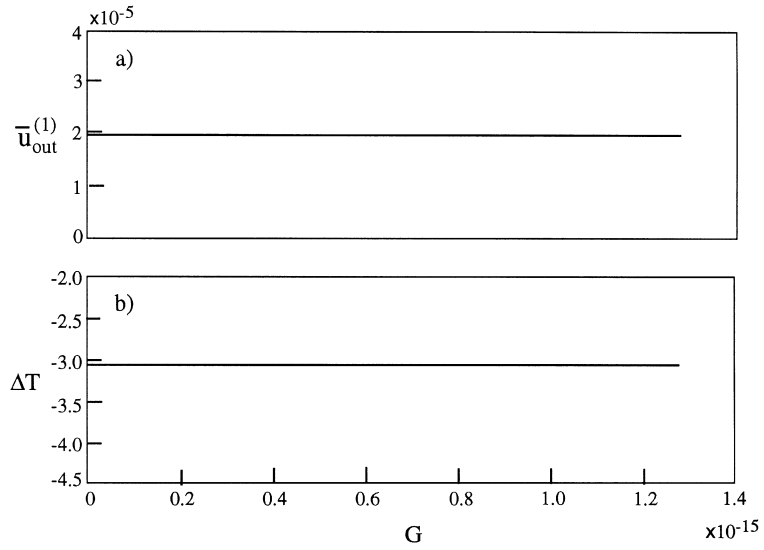


Fig. 14. The effect of gravity on vapor velocity and temperature in the outlet cross-section of the capillary. (a) the dependence of $u^{(1)}(g)$; (b) the dependence of $\Delta T(g)$.

Then we have

$$T_{\mathrm{w}}^{\max} = T_{\mathrm{out}}^{(1)} + q/\alpha \tag{40}$$

where $T_{\mathrm{w}}^{\max}$ is the maximum temperature of the wall and $T_{\mathrm{out}}^{(1)}$ is the outlet vapor temperature.

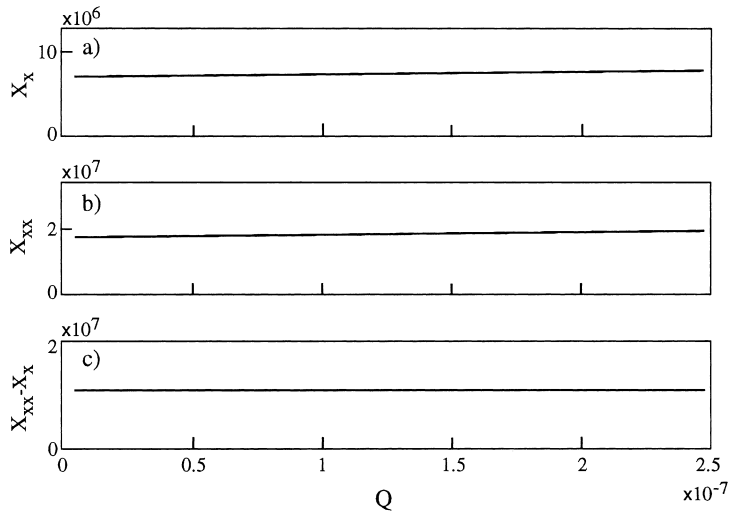


Fig. 15. The effect of wall heat flux on the meniscus position (a) the dependence of $x_*$(q); (b) the dependence of $x_{**}$(q); (c) the dependence of $\Delta X_{**}$(q).

Recalling that $Nu = ARe^n Pr^m$ ($Nu$ and $Pr$ are Nusselt and Prandtl numbers, $A$, $n$, $m$ are known constants), we rewrite Eq. (39) in the following form

$$T_w^{\max} = T_{out}^{(1)} + cq \tag{41}$$

where $c = (D^{1-n}\nu^n/\lambda A V^n P_r^m)$, where $\lambda$ is the thermal conductivity and $\nu$ is the kinematic viscosity.

Let the permissible wall temperature equal $T_{w.p.}$ Then we obtain the following estimation for the permissible heat flux on the wall $q_p$.

$$cq_p \le T_{w.p.} - T_{out}^{(1)} \tag{42}$$

The inequality (42) gives an estimation on the limiting permissible value of heat flux on the wall.

## 9. Conclusion

The quasi-one-dimensional model of flow in a heated microchannel used in the present research makes it possible to describe the fundamental features of two-phase capillary flow due to the heating and evaporation of the liquid. The approach developed allows the estimation of the effects of capillary, inertia, frictional and gravity forces on the shape of the interface surface as well as the velocity and temperature distributions. The results of the numerical solution of the system of one-dimensional mass momentum and energy conservation equations,

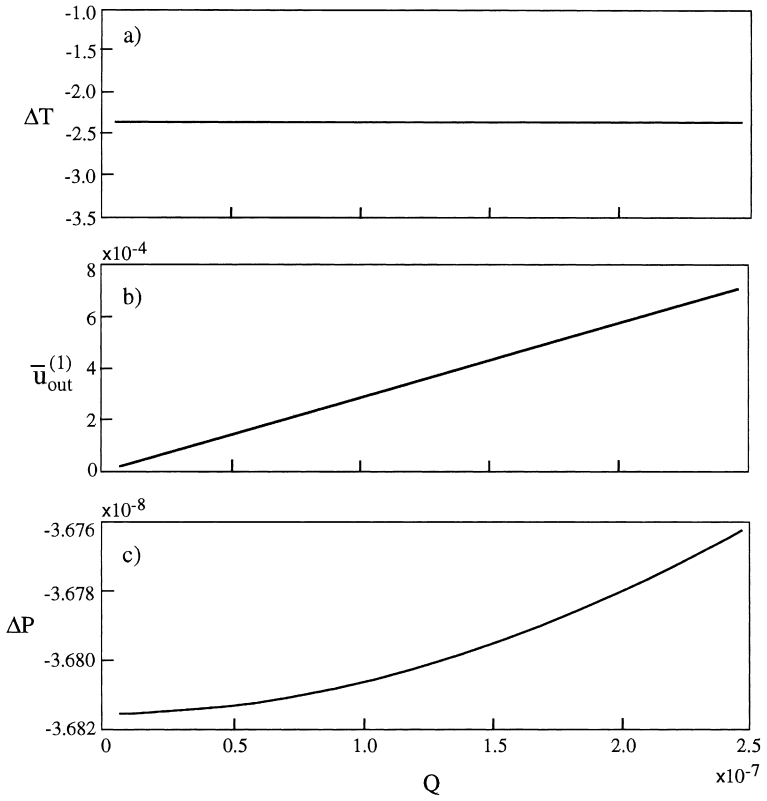


Fig. 16. The dependencies of the vapor temperature, pressure and the velocity in the outlet cross-section of the capillary on the wall heat flux (a) the dependence of $\Delta T(q)$; (b) the dependence of $u^{(1)}(q)$; (c) the dependence of $\Delta p(q)$.

a detailed analysis of the hydrodynamic and thermal characteristic of the flow in heated capillary with evaporative interphase surface are carried out.

The following results have been obtained.

1. The velocity, pressure and temperature distribution in a heated capillary with evaporative interphase surface are determined by the following parameters accounting the physical properties of the liquid and vapor as well as hydrodynamic and thermal conditions of the flow: the Reynolds, Euler, Peclet, Froude and Weber numbers and four non-dimensional groups $\gamma$, $\Omega$, $\omega$ and $\vartheta$.
2. The vapor pressure, density and temperature practically do not change along the evaporation region in physically realistic systems. The latter allows to simplify the system of governing equations and reduce the problem to successive solution of the shortened system of equations to determine the velocity, liquid pressure and gaseous phases as well as the interphase shape in a heated capillary.

3. The difference in pressure between vapor and liquid within the evaporation region depends mainly on the Euler and Weber numbers as well as on the thermal parameter $\vartheta$. The effect of the Reynolds and Froude numbers on the difference of both phases pressure is negligible.
4. The curvature of the meniscus in a heated capillary with evaporative interphase surface is not constant.
5. Increasing the initial liquid temperature is accompanied by a change of the length of the liquid and vapor regions, the increase of the vapor velocity and temperature as well as the total drag in the microchannel.
6. Heatflux on the wall, gap-size of capillary as well as gravity affects noticeably the total drag of microchannel and temperature difference between the inlet and outlet cross-sections.
7. At Euler number larger than $10^8$ a self regulated regime of flow is realized at which the length of heating, evaporation and super heating regions as well as liquid and vapor temperatures do not depend on the wall heat flux. At such flow the wall temperature depends on the liquid (vapor) temperature, heat transfer intensity and wall heat flux.
8. The maximum possible heat flux which corresponds to the maximum allowed wall temperatures is estimated. This maximum wall heat flux is determined by the difference between the permissible wall temperature and the vapor temperature in the outlet cross-section which is a function of the Reynbolds and Nusselt numbers.

## Acknowledgements

This work was supported by the Ministry of Science and the Arts (State of Israel). L.P.Y. is supported by the Israel Council for higher Education.

## Appendix A

The vapor and liquid densities, pressure and temperature on the interface surface are connected by the following equation (Carey, 1992):

$$\frac{1}{\rho^{(1)}}\frac{\mathrm{d}P^{(1)}}{\mathrm{d}T}+\frac{1}{\rho^{(2)}}\frac{\mathrm{d}P^{(2)}}{\mathrm{d}T}=\frac{h_{\mathrm{LG}}}{T} \tag{A.1}$$

where $h_{\mathrm{LG}}$ is the latent heat of evaporation.

On the meniscus surface the deviation of vapor pressure $P^{(1)}$ from the saturation pressure $P_{\mathrm{s}}$ depends on the surface tension $\beta$, liquid density $\rho^{(2)}$, gas constant $R$, temperature $T$ and radii of curvature $r$. When $P^{(1)}-P_{\mathrm{sat}}(T)\ll(2\beta/r_2)$ (which is usually the case), $P^{(1)}$ can be approximated for most systems (Carey, 1992) by: $P^{(1)}=P_{\mathrm{sat}}\exp(-(2\beta/RT\rho^{(2)}r_2))$. When the ratio $2\beta/RT\rho^{(2)}r^{(2))}\ll1$, it is possible to assume $P^{(1)}=P_{\mathrm{s}}$.

In this case the vapor pressure on the interface surface may be found from the Clapeyron–Clausius equation

$$\frac{\mathrm{d}P^{(1)}}{\mathrm{d}T^{(1)}}=\frac{h_{\mathrm{LG}}\rho^{(1)}}{T^{(1)}} \tag{A.2}$$

## Appendix B

Let us transform Eqs. (14)–(16) using Gauss' theorem

$$\int_{v^{(\alpha)}} \frac{\partial}{\partial x_l}(\rho^{(\alpha)} v_l^{(\alpha)})\,\mathrm{d}v = \int_{\Sigma^{(\alpha)}} \rho^{(\alpha)} v_l^{(\alpha)}\,\mathrm{d}\mathbf{S}_l \tag{B.1}$$

$$\int_{v^{(\alpha)}} \frac{\partial}{\partial x_l}\left[(\rho^{(\alpha)} v_l^{(\alpha)} h^{(\alpha)}) - \lambda^{(\alpha)} \frac{\partial T^{(\alpha)}}{\partial x_l}\right]\mathrm{d}v = \int_{\Sigma^{(\alpha)}} \left[(\rho^{(\alpha)} v_l^{(\alpha)} h^{(\alpha)}) - \lambda^{(\alpha)} \frac{\partial T^{(\alpha)}}{\partial x_l}\right]\mathrm{d}\mathbf{S}_l \tag{B.2}$$

$$\int_{v^{(\alpha)}} \frac{\partial}{\partial x_k}(\Pi_{ik}^{(\alpha)})\,\mathrm{d}v = \int_{\Sigma^{(\alpha)}} \Pi_{ik}^{(\alpha)}\,\mathrm{d}\mathbf{S} \tag{B.3}$$

where $\Sigma^{(\alpha)}$ and $v^{(\alpha)}$ are the surface and the volume of the vapor and liquid media, respectively; $\mathbf{S}_k = n_k S$, $\mathbf{S}_l = n_l S$. $n_k\,(n_l)$ is the external normal to that surface.

The integrals $\int_{\Sigma^{(1)}} A^{(1)}\,\mathrm{d}\mathbf{S}_k$ and $\int_{\Sigma^{(2)}} A^{(2)}\,\mathrm{d}\mathbf{S}_k$

$$(A^{(\alpha)} = \rho^{(\alpha)} v_l^{(\alpha)}, \rho^{(\alpha)} v_l^{(\alpha)} h^{(\alpha)}, \lambda^{(\alpha)} \nabla T_l^{(\alpha)}, \Pi_{ik}^{(\alpha)})$$

are equal (see Fig. 1b)

$$\int_{\Sigma^{(2)}} A^{(2)}\,\mathrm{d}\mathbf{S}_k = \sum_{m=\mathrm{I}}^{\mathrm{viii}} \int_m A^{(2)}\,\mathrm{d}\mathbf{S}_k \tag{B.4}$$

$$\int_{\Sigma^{(1)}} A^{(1)}\,\mathrm{d}\mathbf{S}_k = \sum_{m=\mathrm{I}}^{\mathrm{iii}} \int_m A^{(1)}\,\mathrm{d}\mathbf{S}_k \tag{B.5}$$

where $m$ is the number of restricted surface elements.

Summing integrals (B.4) and (B.5) and accounting:

1. impenetrability of the capillary walls

$$\left(\int_{\mathrm{II}} \rho^{(2)} v^{(2)}\,\mathrm{d}\mathbf{S} = \int_{\mathrm{vii}} \rho^{(2)} v^{(2)}\,\mathrm{d}\mathbf{S} = 0; \int_{\mathrm{II}} \rho^{(2)} v^{(2)} h^{(2)}\,\mathrm{d}\mathbf{S} = \int_{\mathrm{vii}} \rho^{(2)} v^{(2)} h^{(2)}\,\mathrm{d}\mathbf{S} = 0\right);$$

2. adhesion of fluid to the wall

$$\left(\int_{\mathrm{II}} \rho^{(2)} u^{(2)}\,\mathrm{d}\mathbf{S} = \int_{\mathrm{vii}} \rho^{(2)} u^{(2)}\mathbf{S} = 0\right);$$

3. equality

$$\int_{\mathrm{II}} P^{(2)}\,\mathrm{d}\mathbf{S} + \int_{\mathrm{vii}} P^{(2)}\,\mathrm{d}\mathbf{S} = 0;$$

4. opposed signs of the normal to the interface surface on the liquid side and on the vapor side ($n_{\mathrm{i}}^{(1)} = -n_{\mathrm{i}}^{(2)}$) yields (using conditions (6)–(8)) the following equations[5]

$$\sum_{\alpha=1}^{2} \int_{f^{(\alpha)}} \rho^{(\alpha)} u^{(\alpha)}\,\mathrm{d}\mathbf{S} = c_1 \tag{B.6}$$

$$\sum_{\alpha=1}^{2} \int_{f^{(\alpha)}} \left(\rho^{(\alpha)} u^{(\alpha)} h^{(\alpha)} - \lambda^{(\alpha)} \frac{\partial T^{(\alpha)}}{\partial x}\right) \mathrm{d}\mathbf{S} = Q_{\mathrm{ext}} + c_2 \tag{B.7}$$

$$\left(\sum_{\alpha=1}^{2} \int_{f^{(\alpha)}} (\rho^{(\alpha)} u^{(\alpha)^2} + \rho^{(\alpha)} u^{(\alpha)} v^{(\alpha)} + P^{(\alpha)} - \sigma_{xk})\,\mathrm{d}\mathbf{S}\right) + \int_{f_{\mathrm{int}}} \left[\beta(r_1^{-1} + r_2^{-1}) n_i^{(2)} + \frac{\partial \beta}{\partial x_i}\right] \mathrm{d}\mathbf{S} = F_{\mathrm{ext}} + c_3 \tag{B.8}$$

$$\int_{f^{(\alpha)}} \rho^{(\alpha)} u^{(\alpha)}\,\mathrm{d}\mathbf{S} = -\int_{f_{\mathrm{int}}} \rho^{(\alpha)} v_l^{(\alpha)}\,\mathrm{d}\mathbf{S} = c_4 \tag{B.9}$$

$$\int_{f^{(\alpha)}} \left(\rho^{(\alpha)} u^{(\alpha)} h^{(\alpha)} - \lambda^{(\alpha)} \frac{\partial T^{(\alpha)}}{\partial x}\right) \mathrm{d}\mathbf{S} + \int_{f_{\mathrm{int}}} \left(\rho^{(\alpha)} v_l^{(\alpha)} h^{(\alpha)} - \lambda^{(\alpha)} \frac{\partial T^{(\alpha)}}{\partial x_l}\right) \mathrm{d}\mathbf{S} = Q_{\mathrm{ext}} = c_5 \tag{B.10}$$

$$\int_{f^{(\alpha)}} (\rho^{(\alpha)} u^{(\alpha)^2} + \rho^{(\alpha)} u^{(\alpha)} v^{(\alpha)} + P^{(\alpha)} - \sigma_{xk}^{(\alpha)})\,\mathrm{d}\mathbf{S} + \int_{f_{\mathrm{int}}} (\rho^{(\alpha)} v_i^{(\alpha)} v_k^{(\alpha)} + P^{(\alpha)} - \sigma_{ik})\,\mathrm{d}\mathbf{S} = F_{\mathrm{ext}}^{(\alpha)} + c_6 \tag{B.11}$$

where $f^{(\alpha)} = f_{\mathrm{iii}'}$, $2f_{\mathrm{iii}}$; $f_{\mathrm{int}} = 2f_{\mathrm{iv}}$; $\sigma_{xk}^{(\alpha)} = \mu^{(\alpha)}((\partial u^{(\alpha)}/\partial y) + (\partial v^{(\alpha)}/\partial x) - (4/3)\,div\,\mathbf{v})$; $Q_{\mathrm{ext}} = 2\lambda^{(2)} \int_{f_{\mathrm{ii}}} (\partial T^{(2)}/\partial y)\,\mathrm{d}S$; $F_{\mathrm{ext}} = 2\mu^{(2)} \int_{f_{\mathrm{ii}}} \sigma_{yk}^{(2)}\,\mathrm{d}S$; $\sigma_{\mathrm{yk}}^{(\alpha)} = \mu^{(\alpha)}((\partial \mathrm{v}/\partial \mathrm{x}) + (\partial \mathrm{u}/\partial \mathrm{y}) - (4/3)\,\mathrm{d}iv\,\mathbf{v})$; $Q_{\mathrm{ext}}^{(\alpha)} = 0$ at $\alpha = 1$; $Q_{\mathrm{ext}}^{(\alpha)} = Q_{\mathrm{ext}}$ at $\alpha = 2$; $F_{\mathrm{ext}}^{(\alpha)} = 0$ at $\alpha = 1$ constants $c_1$, $c_2$, $c_3$, $c_4$, $c_5$ and $c_6$ correspond to $2\int_{f_{\mathrm{i}}} A^{(2)}\,\mathrm{d}S$; since integrals $\int_{f^{(\alpha)}} \rho^{(\alpha)} u^{(\alpha)} v^{(\alpha)}\,\mathrm{d}S = 0$; $\int_{f^{(\alpha)}} (\partial u/\partial y)\,\mathrm{d}S = \int_{f^{(\alpha)}} (\partial v/\partial y)\,\mathrm{d}S = 0$; $\int_{f_{\mathrm{ii}}} (\partial u/\partial x)\,\mathrm{d}S = \int_{f_{\mathrm{ii}}} (\partial v/\partial x)\,\mathrm{d}S = 0$.

Eqs. (B.8) and (B.11) may be presented as[6]

$$\left(\sum_{\alpha=1}^{2} \int_{f^{(\alpha)}} (\rho^{(\alpha)} u^{(\alpha)^2} + P^{(\alpha)} - \tilde{\sigma}_{xk}^{(\alpha)})\,\mathrm{d}S\right) + \int_{f_{\mathrm{int}}} \left(\beta\psi n_i^{(2)} + \frac{\partial \beta}{\partial x_i}\right) \mathrm{d}S = F_{\mathrm{ext}} + c_3 \tag{B.12}$$

[5] For the plane problem.
[6] Using correlation (10).

$$\int_{f^{(\alpha)}} (\rho^{(\alpha)} u^{(\alpha)^2} + P^{(\alpha)} - \tilde{\sigma}_{xk}^{(\alpha)}\,\mathrm{d}S + \int_{f_{\mathrm{int}}} (\rho^{(\alpha)} v_i^{(\alpha)} v_k^{(\alpha)} + P^{(\alpha)} - \sigma_{ik})\,\mathrm{d}S = F_{\mathrm{ext}}^{(\alpha)} + c_6 \tag{B.13}$$

where $\tilde{\sigma}_{xk} = \mu^{(\alpha)}((\partial v^{(\alpha)}/\partial x) - (4/3)(\partial u^{(\alpha)}/\partial x))$; $F_{\mathrm{ext}} = 2\mu^{(2)} \int_{f_{ii}} ((\partial u^{(2)}/\partial y) - (4/3)(\partial v^{(2)}/\partial y))\,\mathrm{d}S$

Let us introduce average (over the flow cross-section) parameters as:

$$\langle J^{(\alpha)} \rangle = f^{(\alpha)^{-1}} \int_{f^{(\alpha)}} J^{(\alpha)}\,\mathrm{d}S \tag{B.14}$$

where $J$ is under examination parameter and $\langle\ \rangle$ is an operator indicating an averaging over the cross-section. Then Eqs.(B.6), (B.7), (B.9), (B.10), (B.12) and (B.13) transform to the following form:

$$\sum_{\alpha=1}^{2} f^{(\alpha)} \langle \rho^{(\alpha)} u^{(\alpha)} \rangle = c_1 \tag{B.15}$$

$$\sum_{\alpha=1}^{2} f^{(\alpha)} \left( \langle \rho^{(\alpha)} u^{(\alpha)} h^{(\alpha)} \rangle - \lambda^{(\alpha)} \langle \frac{\partial T^{(\alpha)}}{\partial x} \rangle \right) = Q_{\mathrm{ext}} + c_2 \tag{B.16}$$

$$\left( \sum_{\alpha=1}^{2} f^{(\alpha)} \left( \langle \rho^{(\alpha)} u^{(\alpha)} \rangle^2 + \langle P^{(\alpha)} \rangle - \langle \sigma_{xk}^{(\alpha)} \rangle \right) \right) + \int_{f_{\mathrm{int}}} \left( \beta \psi n_i^{(2)} + \frac{\partial \beta}{\partial x_i} \right) \mathrm{d}S = F_{\mathrm{ext}} + c_3 \tag{B.17}$$

$$f^{(\alpha)} \langle \rho^{(\alpha)} u^{(\alpha)} \rangle = - \int_{f_{\mathrm{int}}} \rho^{(\alpha)} v_\ell^{(\alpha)}\,\mathrm{d}S + c_4 \tag{B.18}$$

$$f^{(\alpha)} \left( \langle \rho^{(\alpha)} u^{(\alpha)} h^{(\alpha)} \rangle - \lambda^{(\alpha)} \langle \frac{\partial T^{(\alpha)}}{\partial x} \rangle \right) + \int_{f_{\mathrm{int}}} \left( \rho^{(\alpha)} v_l^{(\alpha)} h^{(\alpha)} - \lambda \frac{\partial T^{(\alpha)}}{\partial x_l} \right) \mathrm{d}S = Q_{\mathrm{ext}}^{(\alpha)} + c_5 \tag{B.19}$$

$$f^{(\alpha)} (\langle \rho^{(\alpha)} u^{(\alpha)2} \rangle + \langle P^{(\alpha)} \rangle - \langle \tilde{\sigma}_{xk}^{(\alpha)} \rangle) + \int_{f_{\mathrm{int}}} (\rho^{(\alpha)} v_i^{(\alpha)} v_k^{(\alpha)} + P^{(\alpha)} - \sigma_{ik})\,\mathrm{d}S = F_{\mathrm{ext}}^{(\alpha)} + c_6 \tag{B.20}$$

Equations (B.15)–(B.20) may be presented (after eliminating the constants $c_1$, $c_2$, $c_3$, $c_4$, $c_5$ and $c_6$) in the following form:

$$\frac{\partial}{\partial x} \left( \sum_{\alpha=1}^{2} f^{(\alpha)} \langle \rho^{(\alpha)} u^{(\alpha)} \rangle \right) = 0 \tag{B.21}$$

$$\frac{\partial}{\partial x} \left( \sum_{\alpha=1}^{2} f^{(\alpha)} \left( \langle \rho^{(\alpha)} u^{(\alpha)} h^{(\alpha)} \rangle - \lambda^{(\alpha)} \langle \frac{\partial T^{(\alpha)}}{\partial x} \rangle \right) \right) = \frac{\partial}{\partial x} Q_{\mathrm{ext}} \tag{B.22}$$

$$\frac{\partial}{\partial x}\left(\sum_{\alpha=1}^{2} f^{(\alpha)}(\langle\rho^{(\alpha)}u^{(\alpha)^2}\rangle + P^{(\alpha)} - \langle\tilde{\sigma}_{xk}^{(\alpha)}\rangle)\right) = \frac{\partial}{\partial x}F_{\text{ext}} - \frac{\partial}{\partial x}F_{\text{int}} \tag{B.23}$$

$$\frac{\partial}{\partial x}(f^{(\alpha)}\langle\rho^{(\alpha)}u^{(\alpha)}\rangle) = -\frac{\partial G_{\text{int}}}{\partial x} \tag{B.24}$$

$$\frac{\partial}{\partial x}\left(f^{(\alpha)}\left(\langle\rho^{(\alpha)}u^{(\alpha)}h^{(\alpha)}\rangle - \lambda^{(\alpha)}\langle\frac{\partial T^{(\alpha)}}{\partial x}\rangle\right)\right) = \frac{\partial}{\partial x}Q_{\text{ext}}^{(\alpha)} - \frac{\partial}{\partial x}Q_{\text{int}}^{(\alpha)} \tag{B.25}$$

$$\frac{\partial}{\partial x}(f^{(\alpha)}(\langle\rho^{(\alpha)}u^{(\alpha)}\rangle + \langle P^{(\alpha)}\rangle - \langle\tilde{\sigma}_{xk}^{(\alpha)}\rangle)) = \frac{\partial}{\partial x}F_{\text{ext}}^{(\alpha)} - \frac{\partial}{\partial x}F_{\text{int}}^{(\alpha)} \tag{B.26}$$

where $F_{\text{int}} = \int_{f_{\text{int}}}(\beta\psi n_i^{(2)} + (\partial\beta/\partial x_i))\,\mathrm{d}S$; $Q_{\text{int}}^{(\alpha)} = \int_{f_{\text{int}}}(\rho^{(\alpha)}v_l^{(\alpha)}h^{(\alpha)} - \lambda^{(\alpha)}(\partial T^{(\alpha)}/\partial x_l))\,\mathrm{d}S$; $F_{\text{int}}^{(\alpha)} = \int_{f_{\text{int}}}(\rho^{(\alpha)}v_\ell^{(\alpha)}v_k^{(\alpha)} + P^{(\alpha)} - \sigma_{ik})\,\mathrm{d}S$ and $G_{\text{int}} = \int_{f_{\text{int}}}\rho^{(\alpha)}v_l^{(\alpha)}\,\mathrm{d}S$.

## Appendix C

We now consider the case where axial heat transfer due to the temperature gradient is negligible compared to the heat transfer from the capillary wall and the friction caused by the velocity gradient in the $x$ direction is negligible compared to the momentum losses at the fluid/wall interface.

### *C.1. Liquid heating region* $0 < \bar{x} < \bar{x}_*$

Equations (18)–(20) contain the following integrals:

$$\bar{\rho}^{(2)}\bar{u}^{(2)} = c_1 \tag{C.1}$$

$$\bar{\rho}^{(2)}\bar{u}^{(2)}h^{(2)} = \vartheta\bar{x} + c_2 \tag{C.2}$$

$$\bar{\rho}^{(2)}\bar{u}^{(2)^2} + Eu\bar{P}^{(2)} = \bar{F}_{\text{ext}} + Fr^{-1}\bar{\rho}^{(2)}\bar{x} + c_3 \tag{C.3}$$

The constants $c_1$, $c_2$ and $c_3$ are found from conditions[7]

$$\bar{x} = 0, \quad \bar{\rho}^{(2)} = 1, \quad \bar{u}^{(2)} = 1, \quad h^{(2)} = 1 \tag{C.4}$$

To determine $\bar{F}_{\text{ext}}$ in Eq. (C.3) we use the relation $f_{\text{ii}} = |k|\int_{x_{\text{in}}}^{x}$ x and $F_{\text{ext}} = \int_{f_{\text{ii}}} t\,\mathrm{d}s$. Assuming $\zeta = 32/Re$ we arrive at

$$\bar{F}_{\text{ext}} = 32/Re\bar{x} \tag{C.5}$$

[7] $c_1 = 1$, $c_2 = 1$, $c_3 = 1 + Eu$.

Then the system of Eqs. (C.1)–(C.3) may be written as

$$\bar{\rho}^{(2)}\bar{u}^{(2)} = 1 \tag{C.6}$$

$$\bar{T}^{(2)} = 1 + \vartheta\bar{x} \tag{C.7}$$

$$(\bar{u}^{(2)} - 1) + Eu(\bar{P}^{(2)} - 1) = -\bar{x}(32/Re + \bar{\rho}^{(2)}/Fr) \tag{C.8}$$

The heating region length is determined from the conditions

$$\bar{x} = \bar{x}_*, \quad \bar{P} = \bar{P}_s, \quad \bar{T} = \bar{T}_s \tag{C.9}$$

Since the dependence $\rho^{(2)} = f(T^{(2)})$ is very weak, it is possible to neglect the liquid density $\rho^{(2)}$ variation within the heating region. Then Eqs. (C.7) and (C.8) may be transformed to:

$$\bar{P}^{(2)} = 1 - (\bar{T}^{(2)} - 1)\Lambda \tag{C.10}$$

where $\Lambda = (32/Re + \bar{\rho}^{(2)}/\varphi Eu)/F_2$

The dependences (C.9) and (C.10) determine the parameters at the end of the heating region. The $\Lambda$ parameter corresponding to micro-cooling system conditions is of the order of $10^{-2}$. In this case $P^*$ and $T^*$ practically do not depend on $\Lambda$. Accordingly, the heating region length depends on the non-dimensional group $\vartheta$ only.

$$\bar{x}_* = (\bar{T}_* - 1)/\vartheta \tag{C.11}$$

### C.2. Evaporation region: $\bar{x}_* \le \bar{x} \le \bar{x}_{**}$

Equations (18)–(22) have the following integrals

$$\sum_{\alpha=1}^{2}(\bar{\rho}^{(\alpha)}\bar{u}^{(\alpha)}\bar{f}^{(\alpha)}) = c_4 \tag{C.12}$$

$$\sum_{\alpha=1}^{2}(\bar{\rho}^{(\alpha)}\bar{u}^{(\alpha)}\bar{f}^{(\alpha)}\bar{h}^{(\alpha)}) = \vartheta\bar{x} + c_5 \tag{C.13}$$

$$\sum_{\alpha=1}^{2}(\bar{\rho}^{(\alpha)}\bar{u}^{(\alpha)^2}f^{(\alpha)}) + Eu\sum_{\alpha=1}^{2}(\bar{P}^{(\alpha)}\bar{f}^{(\alpha)}) = \bar{F}_{\text{ext}} - We^{-1}\int_{\bar{f}_{\text{int}}}\bar{\beta}\bar{\psi}n_i\,\mathrm{d}\mathbf{S} - We^{-1}\int_{\bar{f}_{\text{int}}}\frac{\partial\beta}{\partial\bar{x}_i}\,\mathrm{d}\mathbf{S} + Fr^{-1}\int_{\bar{x}_*}^{\bar{x}}\left(\sum_{\alpha=1}^{2}\bar{\rho}^{(\alpha)}\bar{f}^{(\alpha)}\right)\mathrm{d}\bar{x} + c_6 \tag{C.14}$$

$$\bar{\rho}^{(1)}\bar{u}^{(1)}\bar{f}^{(1)} = -\int_{\bar{x}_*}^{\bar{x}} \bar{\rho}^{(1)}\bar{u}^{(1)}\sqrt{1+(f^{(1)'})^2}d\bar{x} + c_7 \tag{C.15}$$

$$\bar{\rho}^{(1)}\bar{u}^{(1)^2}\bar{f}^{(1)} + Eu\bar{P}^{(1)}\bar{f}^{(1)} = -\int_{\bar{x}_*}^{\bar{x}} (Eu\bar{P}^{(1)} + \bar{\rho}^{(1)}\bar{u}^{(1)^2})\sqrt{1+(f^{(1)'})^2}\mathrm{d}x + Fr \int_{\bar{x}_*}^{\bar{x}} \bar{\rho}^{(1)}\bar{f}^{(1)}d\bar{x} + c_8 \tag{C.16}$$

The constants $c_4$, $c_5$, $c_6$, $c_7$ and $c_8$ are found from the conditions[8]

$$\bar{x} = \bar{x}_*, \quad \bar{f}^{(1)} = 0, \quad \bar{f}^{(2)} = 1, \quad \bar{\rho}^{(\alpha)} = \bar{\rho}_*^{(\alpha)}, \quad \bar{u}^{(\alpha)} = \bar{u}_*^{(\alpha)}, \quad \bar{P}^{(\alpha)} = \bar{P}_*^{(\alpha)}, \quad \bar{h}^{(\alpha)} = \bar{h}_*^{(\alpha)}$$

Then Eqs. (C.12) and (C.13) may be written as

$$\bar{\rho}^{(1)}\bar{u}^{(1)}\bar{f}^{(1)} + \bar{\rho}^{(2)}\bar{u}^{(2)}\bar{f}^{(2)} = 1 \tag{C.17}$$

$$\bar{\rho}^{(1)}\bar{u}^{(1)}\bar{f}^{(1)}\bar{h}^{(1)} + \bar{\rho}^{(2)}\bar{u}^{(2)}\bar{f}^{(2)}\bar{h}^{(2)} = \bar{h}_*^{(1)} + \vartheta(\bar{x}-\bar{x}_*) \tag{C.18}$$

$$(\bar{\rho}^{(1)}\bar{u}^{(1)^2}\bar{f}^{(1)} + \bar{\rho}^{(2)}\bar{u}^{(2)^2}\bar{f}^{(2)} - \bar{\rho}_*^{(2)}\bar{u}_*^{(2)^2}) + Eu(\bar{P}^{(1)}\bar{f}^{(1)} + \bar{P}^{(2)}\bar{f}^{(2)} - \bar{P}_*^{(2)}) = -We^{-1} \int_{f_{\mathrm{int}}} \bar{\beta}\bar{\psi}n_i d\bar{S} - We^{-1}\int_{\bar{f}_{\mathrm{int}}} \frac{\partial\bar{\beta}}{\partial\bar{x}_i}d\bar{S} - 32/Re(\bar{x}-\bar{x}_*) - Fr^{-1}\int_{\bar{x}_*}^{\bar{x}} \left(\sum_{\alpha=1}^{2}\bar{\rho}^{(\alpha)}\bar{f}^{(\alpha)}\right)\mathrm{d}\bar{x} \tag{C.19}$$

$$\bar{\rho}^{(1)}\bar{u}^{(1)}\bar{f}^{(1)} = \int_{\bar{x}_*}^{\bar{x}} \bar{\rho}^{(1)}\bar{u}^{(1)}\sqrt{1+(f^{(1)'})^2}\,\mathrm{d}\bar{x} \tag{C.20}$$

$$\bar{\rho}^{(1)}\bar{u}^{(1)^2}\bar{f}^{(1)} + Eu\bar{P}^{(1)}\bar{f}^{(1)} = \int_{\bar{x}_*}^{\bar{x}} (Eu\bar{P}^{(1)} + \bar{\rho}^{(1)}\bar{u}^{(1)^2})\sqrt{1+(f^{(1)'})^2}\mathrm{d}\bar{x} - Fr^{-1}\int_{\bar{x}_*}^{\bar{x}} \bar{\rho}^{(1)}\bar{f}^{(1)}\,\mathrm{d}\bar{x} \tag{C.21}$$

The left hand side of Eq. (C.18) can be presented as:

$$\bar{\rho}^{(1)}\bar{u}^{(1)}\bar{f}^{(1)}\bar{h}^{(1)} - \bar{\rho}^{(1)}\bar{u}^{(1)}\bar{f}^{(1)}\bar{h}^{(2)} + \bar{\rho}^{(1)}\bar{u}^{(1)}\bar{f}^{(1)}\bar{h}^{(2)} + \bar{\rho}^{(2)}\bar{u}^{(2)}\bar{f}^{(2)}\bar{h}^{(2)}$$

$$= \bar{\rho}^{(1)}\bar{u}^{(1)}\bar{f}^{(1)}(\bar{h}^{(1)} - \bar{h}^{(2)}) + \bar{h}^{(2)}(\bar{\rho}^{(1)}\bar{u}^{(1)}\bar{f}^{(1)} + \bar{\rho}^{(2)}\bar{u}^{(2)}\bar{f}^{(2)}) = \bar{\rho}^{(1)}\bar{u}^{(1)}\bar{f}^{(1)}(\bar{h}^{(1)} - \bar{h}^{(2)}) + \bar{h}^{(2)}$$

Then Eq. (C.18) has form

$$\bar{\rho}^{(1)}\bar{u}^{(1)}\bar{f}^{(1)}(\bar{h}^{(1)} - \bar{h}^{(2)}) + \bar{h}^{(2)} = \bar{h}_*^{(2)} + \vartheta(\bar{x}-\bar{x}_*) \tag{C.22}$$

[8] $c_4 = 1$, $c_5 = h_*^{(1)} - \vartheta\bar{x}_*$, $c_6 = Eu\bar{P}_*^{(2)} + \bar{\rho}_*^{(2)}u_*^{(2)^2} - 32/Re\bar{x}_*$, $c_7 = 0$, $c_8 = 0$.

If $\bar{h}^{(\alpha)}=\bar{c}_p^{(\alpha)}\bar{T}(\bar{c}_p^{(2)}=1)$ then[9]

$$\bar{T}=(1+\bar{q}_{ev}\bar{\rho}^{(1)}\bar{u}^{(1)}\bar{f}^{(1)})^{-1}[\bar{T}_*+\vartheta(\bar{x}-\bar{x}_*)] \tag{C.23}$$

where $\bar{q}_{ev}=q_{ev}/c_{p_{20}}T_{20}$.

The location of $\bar{x}_{**}$ can be determined from the conditions[10]

$$\bar{x}=\bar{x}_{**},\quad \bar{f}^{(1)'}=tg\Theta\quad(\bar{f}^{(1)}=1) \tag{C.24}$$

where $\Theta$ is the contact angle.

At a given Weber number, condition (C.24) may be satisfied at some values of Euler number which play role of eigenvalues.

The second integral in right hand side of Eq. (C.19) may be presented as

$$\int_{\bar{f}_{\rm int}}\frac{\partial\bar{\beta}}{\partial\bar{x}_i}\,\mathrm{d}\bar{S}=\int_{\bar{f}_{\rm int}}\frac{\partial\bar{\beta}}{\partial\bar{T}}\frac{\partial\bar{T}}{\partial\bar{x}_i}\,\mathrm{d}\bar{S} \tag{C.25}$$

where $(\partial\bar{\beta}/\partial\bar{T})<0$ for most known liquids.

In the partial case when $\beta$ is constant the first integral in the right hand side of Eq. (C.19) may be expressed as

$$\int_{\bar{f}_{\rm int}}\bar{\beta}\bar{\psi}n_i\,\mathrm{d}\bar{S}=(\text{arc } tg\,\bar{f}^{(1)'}-\pi/2) \tag{C.26}$$

### C.3. Superheat region: ($\bar{f}^{(1)}=1;\ \bar{f}^{(2)}=0$)

Equations (24)–(26) have the following integrals

$$\bar{\rho}^{(1)}\bar{u}^{(1)}=c_9 \tag{C.27}$$

$$\bar{\rho}^{(1)}\bar{u}^{(1)}\bar{h}^{(1)}=\bar{\vartheta}\bar{x}+c_{10} \tag{C.28}$$

$$\bar{\rho}^{(1)}\bar{u}^{(1)^2}+Eu\bar{P}^{(1)}=\bar{F}_{\rm ext}+Fr^{-1}\bar{\rho}^{(1)}\bar{x}+c_{11} \tag{C.29}$$

where the constants $c_9$, $c_{10}$ and $c_{11}$ are found from the conditions

$$\bar{x}=\bar{x}_{**},\quad \bar{\rho}^{(1)}=\bar{\rho}^{(1)}_{**},\quad \bar{u}^{(1)}=\bar{u}^{(1)}_{**},\quad \bar{P}^{(1)}=\bar{P}^{(1)}_{**},\quad \bar{T}^{(1)}=\bar{T}^{(1)}_{**}$$

Then

$$\bar{\rho}^{(1)}\bar{u}^{(1)}=1 \tag{C.30}$$

---

[9] Eq. (C.23) may be presented in the following form $\bar{\rho}^{(1)}\bar{u}^{(1)}\bar{f}^{(1)}=(1+\vartheta\bar{x}-\bar{T}^{(2)})/\bar{q}_{ev}$.

[10] The solution of Eq. (C.19) must satisfy the following conditions: $\bar{x}=\bar{x}_*$, $\bar{f}^{(1)}=\infty$, ($\bar{f}^{(1)}=0$); $\bar{x}=\bar{x}_{**}$ $f^{(1)=tg\Theta}$, ($\bar{f}^{(1)}=1$).

$$\bar{T}^{(1)} = \bar{T}_{**} + \vartheta/\bar{c}_p^{(1)}(\bar{x} - \bar{x}_{**}) \tag{C.31}$$

$$(\bar{u}^{(1)} - \bar{u}_{**}^{(1)}) + Eu(\bar{P}^{(1)} - \bar{P}_{**}^{(1)}) = -32/Re(\bar{x} - \bar{x}_{**}) - Fr^{-1}(\bar{\rho}^{(1)}\bar{x} - \bar{\rho}_{**}^{(1)}\bar{x}_{**}) \tag{C.32}$$

The system of Eqs.(C.1), (C.3), (C.17), (C.21), (C.30) and (C.32) allows us to find the density, velocity, temperature and pressure distributions along the capillary axis, as well as the interface surface shape.

## References


Bailey, D.K., Ameel, T.A., Warrington, R.O., Savoie, T.I., 1995. Single-phase forced convection heat transfer in microgeometries: a review. ASME IECEC paper, ES-396, pp. 301–310.

Bowers, M.B., Mudawar, I., 1994a. High flux boiling in low flowrate, low pressure drop mini-channel and micro-channel heat sink. Int. J. Heat-Mass Transfer 37, 321–332.

Bowers, M.B., Mudawar, I., 1994b. Two-phase electronic cooling using mini channel and micro-channel heat sink. Part 2. Flow rate and pressure drop constraints. J. Electron. Packaging, ASME 116, 298–305.

Carey, V.P., 1992. Liquid–vapour phase-change phenomena. Hemisphere, Washington, Philadelphia, London.

Collier, S.P., 1981. Convective boiling and condensation. McGraw-Hill, New York.

Ha, J.M., Peterson, G.P., 1998. Capillary performance of evaporation flow in micro grooves: an analytical approach for very small tilt angles. ASME J. Heat Transfer 120, 452–457.

Khrustalev, D., Faghri, A., 1995. Fluid flow effect in evaporation from liquid–vapour meniscus. J. Heat Transfer ASME 117, 740–747.

Landau, L.D., Lifshitz, E.M., 1959. Fluid Mechanics, 2nd ed. Pergamon, London.

Landerman, C.S., 1994. Microchannel flow boiling mechanisms leading to Burnout. J. Heat Transfer Electron. Syst. ASME HTD-292, 124–136.

Levich, V.G., 1962. Physicochemical Hydrodynamics. Prentice Hall, London.

Morijama, K., Inoue, A., 1992. The thermohydraulic characteristics of two-phase flow in extremely narrow channels (the frictional pressure drop and heat transfer of boiling two-phase flow, analytical model). Heat Transfer Jpn. Res. 21, 838–856.

Peng, X.F., Peterson, G.P., 1995. The effect of thermodluid and geometrical parameters on convection of liquids through rectangular microchannels. Int. J. Heat-Mass Transfer 38, 755–758.

Peterson, G.P., Ha, J.M., 1998. Capillary performance of evaporation flow in micro grooves: approximate analytical approach and experimental investigation. ASME J. Heat Transfer 120, 743–751.

Smirnov, V.I., 1964. A Course of Higher Mathematics, Vol. II. Pergamon Press, London.

Tuckerman, D.B., Pease, R.F.W., 1981. High-performence heat sinking for VLSI. IEEE Electron Devise Lett. EDL-2, 126–129.

Tuckerman, D., 1984. Heat transfer microstructure for integrated circuits. Ph.D. thesis, Stanford University, Stanford, CA.

Wallis, G.B., 1969. One-dimensional two-phase flow. McGraw-Hill, New York.

Wayner, P.C., Kao, Y.K., LaCroix, L.V., 1976. The interline heat transfer coefficient of an evaporating wetting film. Int. J. Heat Mass Transfer 19, 487–492.

Xu, X., Carey, V.P., 1990. Film evaporation from a micro-grooved surface: an approximate heat transfer model and its comparison with experimental data. J. Thermophys. 4 (4), 512–520.

Weisberg, A., Bau, H.H., Zemel, J.N., 1992. Analysis of microchannels for integrated cooling. Int. J. Heat Mass Transfer 35, 2465–2472.

Wu, P.Y., Little, W.A., 1984. Measurement of the heat transfer characteristics of gas flow a fine channels heat exchangers used for microminiature refrigerators. Cryogenics 24, 415–420.